Journal of Physics B:
Atomic, Molecular and
Optical Physics

TOPICAL REVIEW

Attosecond physics

INSTITUTE OF PHYSICS PUBLISHING JOURNAL OF PHYSICS B: ATOMIC, MOLECULAR AND OPTICAL PHYSICS

J. Phys. B: At. Mol. Opt. Phys. **39** (2006) R1–R37 doi:10.1088/0953-4075/39/1/R01

TOPICAL REVIEW

Attosecond physics

A Scrinzi[1], M Yu Ivanov[2], R Kienberger[3] and D M Villeneuve[2]

[1] Vienna University of Technology, Photonics Institute, Gusshausstrasse 27/387, 1040 Vienna, Austria
[2] National Research Council of Canada, 100 Sussex Drive, Ottawa, ON K1A 0R6, Canada
[3] Max-Planck-Institut für Quantenoptik, Hans Kopfermann Str. 1, D-85748 Garching, Germany

E-mail: Misha.Ivanov@nrc-cnrc.gc.ca, reinhard.kienberger@mpq.mpg.de, scrinzi@tuwien.ac.at and David.Villeneuve@nrc-cnrc.gc.ca

Received 9 August 2005
Published 7 December 2005
Online at stacks.iop.org/JPhysB/39/R1

Abstract

Experiments on the sub-femtosecond time scale performed in recent years and their theoretical background are reviewed in this article. We present the essentials of the generation of attosecond pulses, phase-stabilized few-cycle laser pulses, and applications to sub-femtosecond control of electronic motion and time-resolved spectroscopy of atoms and molecules. An outlook on emerging pulse-generation techniques and time-resolved imaging of electronic and molecular structure is included.

(Some figures in this article are in colour only in the electronic version)

1. Introduction

The typical time scale of electron motion in atoms and molecules is a few hundred attoseconds (1 as $= 10^{-18}$ s)—shorter than any pulse of visible light, shorter even than a single electric field period at optical wavelength. Yet, in several recent experiments it was demonstrated that attosecond electron motion can be controlled by strong short laser pulses [1] and that it can be exploited to directly measure the electric field of a light pulse [2], to obtain an image of an electronic orbital [3], or to produce extreme ultraviolet (XUV) pulses of a few hundred attoseconds duration [4]. The XUV pulses can be timed relative to the laser field with a precision of a few tens of attoseconds, thus opening the route to time-resolved atomic physics [5]. The newly emerging field was dubbed 'attosecond physics'.

This development is based on the ever increasing control over laser pulses. Pulses with durations of a few tens of femtoseconds and intensities around 10^{14} W cm^{-2} are routinely available for wavelengths in the range from 400 nm to 2 μm. Pulses with durations near the limit of a single field oscillation between 800 nm (the Ti:sapphire wavelength) and 1.1 μm can presently be generated at several laboratories [6–12]. For these short pulses intensities approach 10^{18} W cm^{-2} and remarkably low intensity fluctuations of 1% [13] were reported. Not only the pulse envelope, but also the *electric field* of the pulses is highly reproducible and

can be controlled with shot to shot phase fluctuations of less than 100 as [4], fluctuations that make up only small fractions of the Ti:sapphire laser optical period of 2.6 fs.

At high pulse intensity new types of experiments become possible, as the interaction of a strong laser pulse radically differs from light–matter interaction at lower intensities. Rather than accumulating an effect over many optical periods, as in conventional optics, the electric field can take direct control of electronic motion and imprint its time structure on electron momentum and position. Ionization plays an important role for the precise timing of electronic motion in the field because of its strongly nonlinear dependence on electric field strength: the rather smooth sine-like variation of the laser field produces pronounced peaks of electron emission at times near maximum field. The resulting short electron wave packets can be accelerated by the laser and directed back to the parent ion. Upon scattering from the parent ion after roughly one half-cycle of the laser field one obtains a short time snapshot of the ion's nuclear positions [14] or even of its valence electron orbital [3]. When scattering is inelastic, further electrons may be ejected from the ion, which provides information about the electron dynamics half a laser period after ionization [15, 16].

Inelastic scattering may result in the generation of broadband radiation with energies that are proportional to the kinetic energy of the electron at the moment of scattering. As the electron energy varies rapidly during a single laser cycle, a given range of photon energies is generated only during very short times of sub-laser-cycle duration. By applying a spectral filter and compensating chirp one can generate bursts of XUV radiation with durations as short as 170 as [17]. These shortest pulses have the disadvantage of coming in trains with a repetition rate of twice the laser frequency. The presently shortest *isolated* pulse lasts 250 as [4]; that is, $1/10$ of the optical period of the Ti:sapphire laser.

With photon energies of about 100 eV present attosecond XUV pulses can trigger atomic and molecular inner-shell processes, whose dynamics can be monitored by a precisely timed laser pulse. This method was demonstrated by the time-resolved measurement of an Auger decay [5]. The shortest accessible times are, roughly, limited by the XUV pulse duration or, under certain conditions, by its 100 as jitter relative to the laser pulse [18]. Different from direct electron recollision, this type of pump–probe experiment can also monitor times that extend over many laser optical periods.

In the present review, we want to touch upon all essential aspects of attosecond physics: its theoretical foundations, the enabling technology of short pulse generation, and highlights of experimental achievements, as well as the prospects for its future development. It goes without saying that only a few selected topics can be discussed in any detail, while the reader is referred to the literature for both in depth and more complete discussions. Recent reviews on closely related topics include the review on intense few-cycle laser pulses by Brabec and Krausz [9], which has become a standard reference for the field and an excellent overview over high harmonic generation by Agostini and DiMauro [19].

2. Basic theory

Attosecond control of electronic motion is achieved by laser fields that are comparable in strength to the electric field in the atom. At first sight, this creates a rather complex interplay between atomic and laser forces. Fortunately, for the majority of phenomena in attosecond physics, one can separate the dynamics into a domain 'inside' the atom, where atomic forces dominate, and 'outside', where the laser force dominates. Apart from full blown numerical calculations all models of attosecond phenomena rely on this basic picture, be it in a classical, semi-classical, or fully quantum mechanical fashion. It turns out that in many cases the

classical pictures already capture the essence of the phenomena and quantum calculations are only needed to obtain quantitatively correct results.

The laser pulses used are, in general, short from 40 fs duration down to ∼5 fs or about two optical cycles at the wavelength of 800 nm. The fast rise time of the pulses allows one to reach high field strength before the atom or molecule disintegrates. For pulse durations near or below two optical cycles, in addition to the pulse envelope and the carrier frequency, the *carrier–envelope phase* φ_{CE} is a third important parameter to fully characterize the pulse. The electric field of a very short pulse with envelope $\mathcal{E}_0$ and central frequency ω,

$$\mathcal{E}(t) = \mathcal{E}_0(t)\cos(\omega t + \varphi_{\mathrm{CE}}), \tag{1}$$

qualitatively depends on φ_{CE}: for an envelope with its maximum at $t = 0$, a value of $\varphi_{\mathrm{CE}} = 0$ (*'cosine-pulse'*) means that a single field peak significantly exceeds all other field maxima during the pulse, while with $\varphi_{\mathrm{CE}} = \pi/2$ (*'sine-pulse'*) two equally strong field peaks with opposite signs are reached before and after $t = 0$.

2.1. Ionization by strong laser fields

Ionization as the transition from 'inside' to 'outside' the atom plays a key role for attosecond phenomena. A rough distinction is made between single- and multi-photon ionization on the one hand and tunnel and 'barrier-suppression' ionization on the other hand. Multi-photon ionization is a process that extends over several electric field cycles with pronounced interference between electron wavefunction amplitudes produced during each cycle. It is characterized by distinct photoelectron peaks at energies $E_s = (s_0 + s)\omega\hbar - I_p$, $s = 0, 1, \ldots$, where I_p denotes the system's ionization potential and s_0 is the minimum number of photons needed for ionization. Above threshold ionization (ATI), i.e., photoemission at energies with $s > 0$, becomes significant only at higher intensities $\gtrsim 10^{14}$ W cm^{-2}. For tunnel and barrier-suppression ionization interference between contributions from different times plays a minor role for the ionization yield. Total tunnel ionization is the integral over the *static* field ionization rate for the field strength arising during the pulse [20]. The quasi-static ionization yield Y_{qs} for laser field $\mathcal{E}(t)$ is given by

$$Y_{\mathrm{qs}} = 1 - \exp\left\{-\int_{-\infty}^{\infty} \Gamma(t)\,\mathrm{d}t\right\}, \tag{2}$$

where $\Gamma(t)$ is the ionization rate for static field $\mathcal{E}(t)$. Barrier-suppression ionization can also be considered as quasi-static. It differs from tunnel ionization in that field strengths are large enough to allow classical detachment of the electron (figure 1). The boundary between conventional photoionization and quasi-static ionization is determined by the Keldysh parameter $\gamma = \sqrt{2I_p}\omega/\mathcal{E}_0$ [21], where I_p denotes the system's ionization potential $\sqrt{2Ip}/\mathcal{E}_0$, ω designates the laser circular frequency, and $\mathcal{E}_0$ is the peak electric field strength. Here and below we use atomic units where $\hbar$, the electron mass and the unit charge are all set $= 1$. At values $\gamma \gtrsim 1$ one expects predominantly photoionization, while at $\gamma \lesssim 1$ ionization is quasi-static. Clearly, this is not a sharp distinction and for values of $\gamma \approx 1$ characteristics of both mechanisms are present. However, below we will discuss ionization by either high frequency XUV radiation—a clean photoionization process—or by the strong, near-infrared (800 nm) field of present few-cycle laser pulses, where ionization occurs by tunnelling or barrier-suppression.

Tunnel ionization depends on the electric field strength in a strongly nonlinear way. The tunnel ionization rate for the atomic hydrogen ground state is given as [22]

$$\Gamma(\mathcal{E}) = \frac{4}{\mathcal{E}}\exp\left[-\frac{2}{3\mathcal{E}}\right]. \tag{3}$$

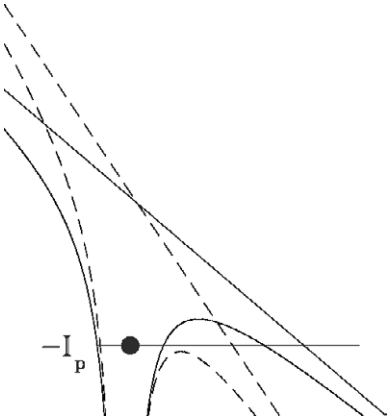

Figure 1. The potential $-1/r - \mathcal{E}r$ for different field strengths. In tunnel ionization (solid line) the ground state energy $-I_p$ remains below the potential barrier. At larger field strength the barrier becomes suppressed (dashed).

A similar formula for general atoms (ADK formula) is widely used to describe tunnel ionization [23]. Recently, the ADK formula was extended to molecules [24]. All these formulae show the characteristic exponential dependence of the ionization rate on the inverse of the field strength. One important consequence of that pronounced nonlinearity is that for tunnelling field strengths most electrons are released at times when the field reaches its peak.

For barrier-suppression field strengths no comparably accurate formulae are known, although promising results were obtained recently for hydrogen [25]. In general, in the barrier-suppression regime one must rely on numerically calculated ionization rates [20, 26–29]. The dependence on field strength is much weaker in this regime, which provides for a broader time distribution of electron release.

Apart from the overall ionization rate, for several applications in attosecond physics it is important to know the distribution of electron momenta 'at the exit of the tunnel', i.e., at some distance from the nucleus, where further electronic motion can be considered as free. A natural choice is the point where electronic motion becomes classically allowed for electrons at the ground state energy (cf figure 1). By looking at the mean energy around the 'exit of the tunnel' one derives zero average initial momentum. The initial momentum distribution in the direction perpendicular to laser polarization can be approximated as follows [30–35]:

$$w(p_\perp) \propto \mathrm{e}^{-p_\perp^2 \sqrt{2I_p}/|\mathcal{E}(t)|}. \tag{4}$$

To derive this expression, only the dominant contributions to tunnelling are included. To the extent that the approximation is applicable it shows that 'all tunnels are alike', i.e., the shape of the wave packet is universal and is only determined by the field strength and the ionization potential. One should keep in mind, however, that these results are obtained in 'exponential accuracy', i.e., only the exponential dependence of the width is reproduced accurately and a multiplicative pre-factor may depend sensitively on details of the initial state. In particular, paper [32] argues that the above expression for $w(p_\perp)$ should be multiplied by the initial bound state in momentum space.

2.2. Photoelectron spectra

The overall characteristics of photoelectron energy spectra generated by atoms in a strong laser pulse can be derived using simple classical arguments. For this one assumes that after

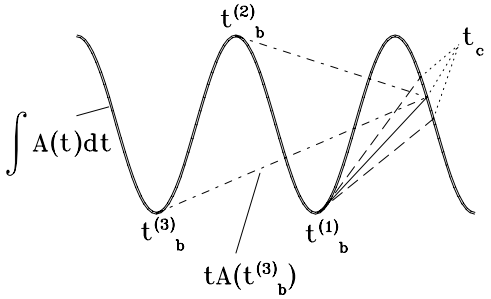

Figure 2. Recollision condition, graphical solution of equation (6). The straight lines connecting release times $t_i^{(i)}$ with recollision time t_c have slopes $A(t_i)$. Recollisions occur where the straight lines intersect with the integral over $A(t)$. A given t_c is reached from several different $t_i^{(i)}$ (dot-dashed and solid lines). The birth time $t_i^{(1)}$ leads to maximum recollision energy. Electrons released slightly before and after $t_i^{(1)}$ recollide later and earlier, respectively, with lower recollision energies ('long' and 'short' trajectories, dashed lines).

the electron has left the atom it moves like a free particle in the laser field, i.e., the ionic potential no longer plays any role. The classical equations of motion are integrated with the initial condition of zero momentum at the time of release t_i, such that the final momentum of an electron after the laser pulse has passed is

$$\vec{p}(t=\infty) = -\int_{t_i}^{\infty} \vec{\mathcal{E}}(t)\,\mathrm{d}t = \vec{A}(t_i). \tag{5}$$

Here $\vec{A}$ is equal to the laser field's vector potential (in Coulomb gauge) up to a factor $1/c$. The maximum energy that can be reached by a photoelectron is solely determined by the maximal vector potential during the laser pulse. For longer pulses that energy is just $2U_p$, where $U_p = A_{\max}^2/4$ is the ponderomotive potential at peak intensity.

The overall shape of observed spectra is determined by the probability for electron release at time t_i, with the highest electron energies $\vec{A}(t_i)^2/2$ for t_i near the peaks of the vector potential. As peaks of the vector potential imply nodes in the field strength, the yield sharply drops with increasing energy. The suppression is exponential in the tunnelling regime because of the exponential decrease of ionization with the inverse field strength (cf equation (3)). In the barrier-suppression regime, where the field strength dependence of the ionization rate is much weaker, high energies are more prominent and one can observe a clear cutoff in electron energies near the maximal energy $2U_p$. The overall shape is modulated by residual interference effects from electron emission at different times.

There is a small but non-negligible likelihood for an electron released at time t_i to be directed back by the laser field and collide with the ion at time t_c: $\vec{r}(t_i) \approx \vec{r}(t_c)$. Integration of the classical equations of motion for the electron trajectory $\vec{r}(t)$ with the initial condition of zero velocity after ionization leads to the recollision condition

$$\int_{t_i}^{t_c} \vec{A}(t)\,\mathrm{d}t = \vec{A}(t_i)(t_c - t_i). \tag{6}$$

Solutions of this transcendental equation for t_c as a function of t_i are represented graphically in figure 2: a given recollision time t_c is connected to a series of release times t_i, of which due to wave packet spreading the closest time gives the strongest contribution (see also figure 6).

A hard collision of the electron with the ion may reverse the electron momentum, which allows higher final electron momenta to be reached. The maximal electron energy reached by

this mechanism is $10U_p$. The release time for these high energy electrons is no longer near a field node and therefore there is always a pronounced cutoff in the spectra at $10U_p$. The intensity of the high energy electrons is typically 3 to 5 orders of magnitude lower than at energies that can be reached without recollision.

The purely classical picture explains the overall structure of observed electron spectra. It also holds for few-cycle pulses, where the cut-off energies become dependent on the carrier–envelope phase φ_{CE} of the pulse. This effect was used for the first measurement of φ_{CE} [36].

Further details of the structure of electron spectra can be explained, when interferences of several classical paths leading to the same final electron momentum are taken into account (see section 2.4).

2.3. High harmonic generation

High harmonic radiation is generated when electrons that return to the ion, instead of being scattered, recombine to form a neutral atom or molecule. The high harmonic generation process consists of three steps: (1) tunnel or barrier-suppression ionization, (2) acceleration by the laser field and redirection to the ion, and (3) recombination with the ion. The excess energy $\omega = I_p + [A(t_c) - A(t_i)]^2/2$ of the recombination process is released as short wavelength radiation. Release t_i and recollision time t_c are connected by equation (6). The maximum harmonic energy is produced by electrons that are released at ~0.05 optical cycles after peak electric field strength and recollide nearly three quarters of an optical cycle later at 0.05 optical cycles before the second following field node. The maximum energy released—the harmonic cutoff energy—is evaluated to

$$\omega_c \approx I_p + 3.17U_p. \tag{7}$$

As in the case of electron spectra, the classical model of harmonic generation also holds for harmonic generation by few-cycle pulses, but the release and recollision times, as well as the cutoff energy, all become dependent on the carrier–envelope phase φ_{CE}.

The simple classical model does not only correctly describe the maximal harmonic energies, it also fully explains the *time structure* of the emitted radiation. In figure 3 the numerically calculated atomic dipole response is compared with the three-step model introduced above. The time–frequency analysis of the numerical result shows that at any time radiation is generated with exactly the photon energies that are predicted by the recollision model.

The time structure of harmonic emission forms the basis of the generation of attosecond pulses. For a few-cycle pulse as in figure 3 the highest harmonic radiation is emitted only during the single laser cycle where the highest electron recollision energies are reached. In that case, the harmonic spectrum has a smooth, unmodulated cutoff and the cutoff radiation has sub-laser-cycle duration. Correspondingly, only a single high frequency attosecond burst of radiation is emitted. The smoothness of the cutoff and emission of only a single pulse depend on the carrier–envelope phase [37, 38]: when the phase is chosen such that two equally high maxima occur in the recollision energy, *two* attosecond pulses are generated that are separated by half the laser optical period. In the harmonic frequency spectrum the additional time structure appears as a modulation close to the cutoff. Single and double pulse emission occur for phases near (but not exactly at) $\varphi_{CE} = 0$ and $\varphi_{CE} = \pi/2$, respectively [39].

With multi-cycle laser pulses the release and recollision process is repeated periodically, and not a single pulse, but a train of harmonic pulses is generated. The corresponding spectrum is a harmonic spectrum in the strict sense, which has pronounced peaks at odd multiples of the fundamental frequency.

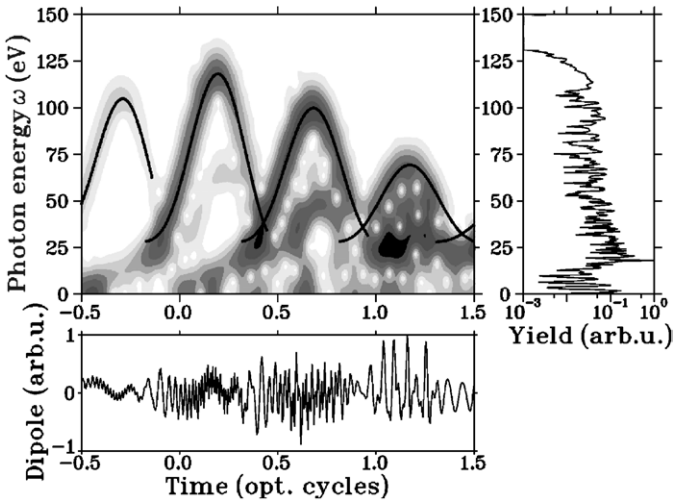

Figure 3. Time–frequency analysis of the dipole response of an atom to a strong few-cycle pulse. The lower panel shows the numerically calculated dipole response. The time–frequency analysis of the signal obtained by Fourier transforming with a Gaussian window function is given in the upper panel. Solid lines indicate the recombination energies obtained by the classical model. Photons with energies ∼120 eV are only emitted during a few hundred attoseconds after $t = 0$. The total harmonic spectrum is shown to the right.

For elliptic polarization recollision becomes suppressed, as it is impossible to fulfil condition (6). This manifests itself in a rapid decrease of high harmonic generation with increasing ellipticity, which was proposed as a mechanism to isolate a single harmonic pulse from a pulse train [40, 41] or to shorten the time of a single recollision [42, 43]. A rapidly time-dependent polarization can be obtained by superimposing fields with two different wavelengths and orthogonal linear polarizations. A first measurement reports the expected behaviour of the spectrum and infers a pulse duration of about 200 as [44]. Elliptically polarized pulses can also be used to determine the background of non-recolliding electrons in a measurement of recollision events (see section 3.1).

The simple and stringent relation between high harmonic frequencies and the generating laser field allows partial reconstruction of the field from the harmonic power spectrum. As phase information is lost in the power spectrum, only time differences can be recovered. It was shown in [39] that the seemingly irregular peak structure of the harmonic spectrum generated by a few-cycle pulse contains information on the height of field peaks in the pulse and the time separation between them. In section 3.2 it will be shown that also detailed information about the wavefunction of the parent ion can be extracted from the harmonic spectrum.

Efficient conversion and the generation of a collimated harmonic beam require phase-matched propagation of fundamental laser pulse and harmonic radiation through the generating medium. Due to the pronounced nonlinearity of the process, computer simulations were needed to theoretically demonstrate the generation of single, smooth attosecond pulses [27]. It turns out that propagation even leads to a 'cleaning' of the harmonic pulses. As can be seen in figure 2, all harmonic energies except the highest ones are generated at least twice during each laser half-cycle, before and after the maximum energy. These energies correspond to the so-called 'short' and 'long' electron recollision trajectories. As a result, the single atom harmonic spectrum (cf figure 3) is rather irregular at lower harmonic frequencies. Depending on whether the laser is focused before or after the atomic gas volume, phase matching favours

contributions from either long or short trajectories [45], leading to a more regular spectrum of harmonic radiation after propagation.

An important effect of propagation is that the harmonic beam is more collimated than the laser beam. The collimated harmonic beam propagates inside the wider laser beam (cf figure 16). This is used in experiments [1, 2, 4, 5, 46] to geometrically separate the two beams.

2.4. Quantum mechanical models

Quantum mechanical models for ATI photoelectron emission, high harmonic generation and attosecond measurements are all based on the so-called strong field approximation, which is the quantum mechanical version of the classical models reviewed above. It carries its name because the laser field is considered as strong compared to the Coulombic field for all but the initial bound state of the system. In these models, the unbound part of the electron wavefunction has the general form [47]

$$\Psi_c(\vec{r},t) = \int \mathrm{d}^3k \int_{-\infty}^{t} \mathrm{d}t'\, \mathrm{e}^{-\mathrm{i}\Phi(\vec{k},t')}\, \mathrm{e}^{\mathrm{i}\vec{k}\cdot\vec{r}}\, \chi(\vec{k},t'), \tag{8}$$

where

$$\Phi(\vec{k},t') = \frac{1}{2}\int_{-\infty}^{t'} [\vec{k} - \vec{A}(\tau)]^2\, \mathrm{d}\tau, \tag{9}$$

is the Volkov phase. The Volkov phase factor times a plane wave gives the Volkov solution for a free electron with canonical momentum $\vec{k}$ in the laser field with vector potential $\vec{A}$ (in velocity gauge). The 'release wavefunction' $\chi(\vec{k},t)$ depends on the electron ionization mechanism. For laser ionization, it is simply [48]

$$\chi(\vec{k},t) = \vec{\mathcal{E}}(t)\cdot\vec{d}(\vec{k})\,\mathrm{e}^{\mathrm{i}I_p t} \tag{10}$$

with the field-free bound–continuum dipole moment $\vec{d}(\vec{k})$.

The integral (8) has a simple intuitive interpretation. The 'release wavefunction' $\chi(\vec{k},t)$ describes how and with which quantum mechanical phase the electron wavefunction is injected into the continuum. The Volkov solution describes its free evolution from that time on and determines how contributions from all times add up. The laser is assumed to only affect the unbound electron motion through the vector potential in the Volkov phase, but has no effect on the release amplitude $\chi(\vec{k},t)$. This limits in practice the applicability of the models described here to moderate laser field strength compared to the fields involved in the dynamics.

The dipole expectation value in the strong field approximation (SFA) is given by

$$\vec{d}_{\mathrm{SFA}}(t) = 2\,\mathrm{Re}\langle\Psi_c|\vec{r}|\Psi_0\rangle, \tag{11}$$

if we assume that the dipole expectation value of the initial state Ψ_0 is $\langle\Psi_0|\vec{r}|\Psi_0\rangle = 0$ and neglect continuum–continuum matrix elements $\langle\Psi_c|\vec{r}|\Psi_c\rangle$. Evaluation of integrals (8) and (11) by stationary phase and saddle-point methods [32] shows that the main contributions come from regions around the classical trajectories, thus establishing the connection between the classical and quantum pictures.

The dominance of a single or a few classical trajectories explains the success of classical models in the description of strong field photoelectron spectra and high harmonic generation [49, 50]. Including a few classical trajectories in the semi-classical picture can explain angular distributions of electron spectra [51], the influence of elliptic polarization [52, 53], or the dependence of electron spectra on ionization potential and laser intensity [54]. Careful analysis of the interference of several trajectories can explain properties of high harmonic generation like coherence [55] or phase matching [56].

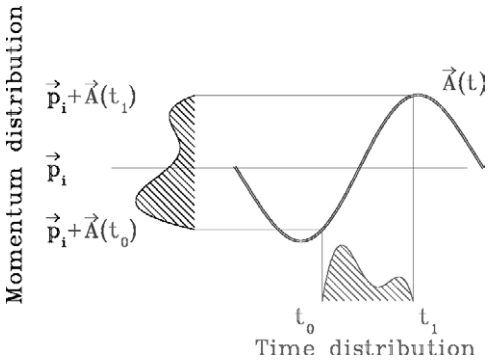

Figure 4. Mapping time distributions into momentum distributions. Electrons are released between times t_0 and t_1 with a certain time-dependent rate and constant initial momentum $\vec{p}_i$. The laser field with vector potential $\vec{A}(t)$ shifts the momenta to different final momenta $\vec{p} = \vec{p}_i + \vec{A}(t)$, depending on the release time t. For clarity, it is assumed that $\vec{p} \parallel \vec{A}(t)\,\forall t$.

The SFA is well suited to describe propagation after electron release. This allows one to recover electron and harmonic spectra in great detail. Tunnel ionization, however, is incorrect in SFA, as neglecting the atomic potential turns out to be a severe approximation. Results obtained in SFA are of 'exponential accuracy', indicating that only the exponential dependence on parameters is rendered correctly, but that multiplicative factors may be incorrect.

There are techniques available to correct SFA for the influence of the ionic potential [57]. With such techniques, quantitatively accurate high harmonic spectra can be obtained [58] and certain asymmetries in electron spectra are explained qualitatively [35].

A variety of other processes can be described in the same framework by choosing a suitable $\chi(\vec{k}, t)$. For laser-dressed XUV ionization with XUV pulse envelope $\vec{\mathcal{E}}_{\mathrm{x}}(t)$ and carrier frequency Ω_{x} one chooses

$$\chi_{\mathrm{x}}(\vec{k}, t) = \vec{\mathcal{E}}_X(t) \cdot \vec{d}(\vec{k})\, \mathrm{e}^{\mathrm{i}(I_p - \Omega_{\mathrm{x}})t}. \tag{12}$$

In the absence of a laser field, inserting equation (12) into (8) leads to the standard photoionization formula with a plane-wave continuum. A similar formula was used to describe the laser-dressed Auger decay [5] with

$$\chi_A(\vec{k}, t) = \sqrt{c_A(t)} q_A(\vec{k})\, \mathrm{e}^{-\mathrm{i}E_A t}, \tag{13}$$

where $c_A(t)$ is the population of the Auger state as given by a rate equation, q_A is the transition matrix element into the continuum, and E_A is the field-free Auger electron energy. Several more processes, like a Fano resonance [59] or multiple resonances [60], can be described with the same type of model.

2.5. Attosecond streaking

An important application of equation (8) is the attosecond streak camera. A classical model is outlined in figure 4. Electrons that are set free in the presence of a dressing laser field are accelerated to different final velocities, depending on their release time. In the simplest case, when the initial momenta are constant during release, the final momentum distribution provides an image of a time-dependent release rate. This case is realized for attosecond XUV photoionization by an unchirped pulse with XUV photon energy Ω_{x}, where one has an initial momentum distribution centred around $|\vec{p}_i| = \sqrt{2(\Omega_{\mathrm{x}} - I_p)}$. The method was generalized to include chirp [61], i.e., a time-dependent $\Omega_{\mathrm{x}}(t)$. Completely general electron

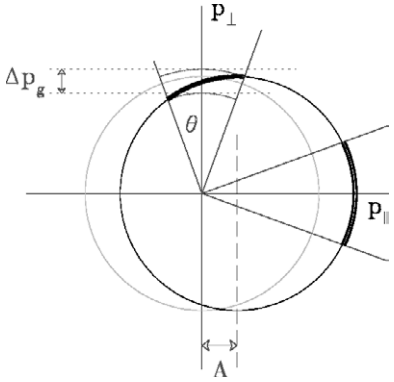

Figure 5. Effects of measurement geometry on electron spectra. An initially isotropic distribution of electron momenta (grey circle) is boosted (black circle) by the vector potential A. When measuring $p_\perp$ perpendicular to laser polarization, a finite acceptance angle θ leads to geometrical broadening Δp_g. The effect is insignificant in the parallel direction $p_\parallel$.

release distributions, which may be generated by more complex release processes, can be recovered by tomographic reconstruction from a set of streaking measurements using the 'atomic transient recorder' [4].

XUV ionization can also be understood as a process that generates an electron wave packet that reflects energy distribution and (initially) also the time structure of the XUV pulse. The time structure is lost during propagation over macroscopic distances because of dispersion, i.e., wave packet spreading. In this picture, the attosecond streak camera takes a snapshot of the electron wave packet at the moment of its release.

In the first attosecond streaking measurements of XUV pulses [46, 62] photoelectrons were measured perpendicular to polarization direction, rather than parallel to polarization as in the example above. With this geometry a finite electron collection angle causes extra broadening of the electron spectra (figure 5). This purely geometrical effect must be taken into account in data analysis.

The classical model breaks down for processes that extend over more than $1/2$ optical period, as electrons released at different times are mapped into the same final momenta and quantum mechanical interference must be taken into account. The quantum mechanical correspondence of a 'release distribution' can be defined and reconstructed by streaking [47]. In the special case of XUV photoionization, reconstruction algorithms developed for FROG measurements can be applied to completely recover the XUV pulse and the laser field from a series of streaking measurements [63].

3. Electron rescattering

In several recent experiments laser-controlled 'microbunches' of electrons were used to obtain images of electronic and nuclear motion in molecules. These experiments exploit the nonlinearity of tunnel ionization to release an electron wave packet at well-defined times near peak laser field strength. An image of the parent ion is taken when the electron wave packet returns some $1/2$ cycle later. The natural time scale of these types of experiments is $\sim 1/2$ optical period, which is 1–2 fs at near-infrared wavelength. Timing can be controlled on the scale of a few hundred attoseconds by varying the laser fundamental frequency. The experiments are performed with moderately strong pulses ($\sim 10^{14}$ W cm^{-2}), which may consist of several optical cycles.

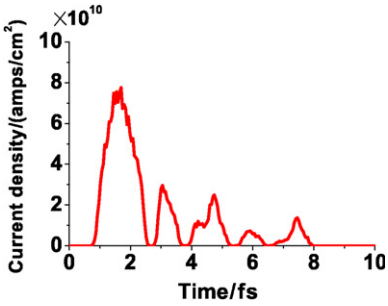

Figure 6. The recollision electron wave packet can be considered as a current pulse when it returns to the parent ion. A semi-classical model is used to estimate the time at which various electron trajectories return. It is converted to an equivalent current density by estimating the lateral size of the wave packet, and defining the current as one unit charge per unit time.

3.1. Time structure of rescattering electrons

One can estimate the temporal shape of the recollision electron wave packet by a semi-classical calculation of electron motion in the presence of both the laser's electric field and the Coulomb potential of the ion [14]. Here we characterize the wave packet as it returns to a parent H_2^+ molecule, since this molecule will be used as a 'molecular clock' to verify the model.

In the calculation, one follows many electron trajectories in two dimensions, each with its own different initial position and velocity, and a weight which reflects the probability of the initial condition. We count the number of trajectories passing through an area corresponding to the inelastic cross section for the $\Sigma_g \rightarrow \Sigma_u$ transition in H_2^+, within a unit time.

In the calculations, the atomic tunnelling rate is corrected for the molecular structure and the influence of the molecular ion's field on the free electron trajectories is included. Figure 6 is a plot of the calculated current density experienced by the molecular ion. Only electrons with energy greater than 15 eV are included in the plotted current density.

Figure 6 shows that the recollision current consists of five microbunches. The first peak has a FWHM duration of 1.2 fs. The current density rises in the second half-period after ionization, reaching 8×10^{10} A cm^{-2}. Such high current densities are available only from very large accelerators such as SLAC. The reason that the current density as seen by the parent ion is so high, is that the photocathode which produces the electron is also the target.

The spread of the electron wave packet in the direction perpendicular to the laser polarization is determined largely by the initial uncertainty of the lateral velocity. It can be measured by introducing ellipticity to the polarization of the laser field. As the amount of ellipticity increases, the electron trajectories are pushed away from the ion, reducing the probability of recollision. An ellipticity of $\epsilon = \mathcal{E}_\perp/\mathcal{E}_\parallel = 0.14$ reduces the recollision probability of H_2 by 1/e, leading to a displacement of 7.7 Å. Thus, the lateral size of the returning wave packet is much larger than the size of most atoms and molecules.

The calculated temporal shape of the electron current can be experimentally verified by using the motion of H_2^+ as a clock. Figure 7 shows the relevant potential energy surfaces of H_2^+. If H_2 is irradiated by a laser with intensity greater than 10^{14} W cm^{-2}, it will be ionized. This will create a vibrational wave packet on the Σ_g electronic surface of H_2^+. For single-photon ionization, the vibrational population distribution of the excited electronic state is determined by the Franck–Condon factors. In the present case of tunnel ionization, the radial dependence of the ionization rate must be considered. It can be seen from figure 7 that the ionization potential to the ground electronic state of H_2^+ decreases with increasing internuclear separation

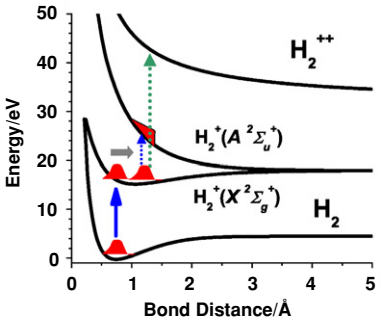

Figure 7. Potential energy diagram for H_2 and H_2^+. The laser will ionize H_2, and the bond will begin to stretch on the H_2^+ σ_g surface. Excitation or ionization will lead to dissociation.

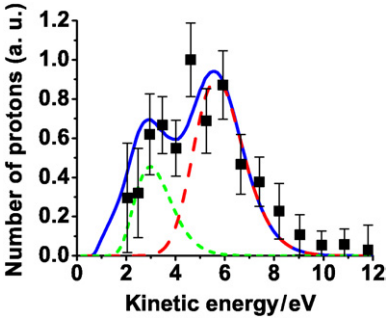

Figure 8. The kinetic energy release per proton is a measure of the time delay between ionization of H_2 and the recollision of the electron. By subtracting the spectrum with elliptically polarized light from that with linearly polarized light, the signal due to recollision can be isolated. The molecular axis was chosen to be perpendicular to the laser polarization to minimize coupling of the surfaces. The experimental points are squares. The dotted lines show the contributions from the first (largest) recollision electron peak and the third peak from the simulation.

R. This leads to preferential ionization of those parts of the ground state vibrational wave packet that have larger R. The effect is that the average internuclear separation for H_2^+ prepared with an intense femtosecond laser is greater than that for a pure vertical transition. This non-Franck–Condon vibrational population in H_2^+ has been observed experimentally [64], and is included in the modelling described herein.

If the returning electron scatters inelastically from the remaining electron in H_2^+, either excitation or ionization will result. In either case, since all excited states of H_2^+ are dissociative, fragmentation will occur. The kinetic energy of the fragments gives a measure of the internuclear separation of the protons at the time of recollision. Thus the motion of the protons on the Σ_g surface acts as a clock that maps the time delay between ionization and recollision [14, 65, 66].

In figure 8 we see the proton kinetic energy distribution. The solid line represents a quantum mechanical simulation assuming a current density as shown in figure 6. The dotted lines show the contributions from the first (largest) peak and the third peak. The agreement between the model and the measurement confirms the accuracy of the calculated current pulse shape in figure 6.

These conclusions are consistent with those of Mairesse *et al* [67]. Their measurement of the emission time of high harmonics implies an electron wave packet pulse duration of about 1.2 fs.

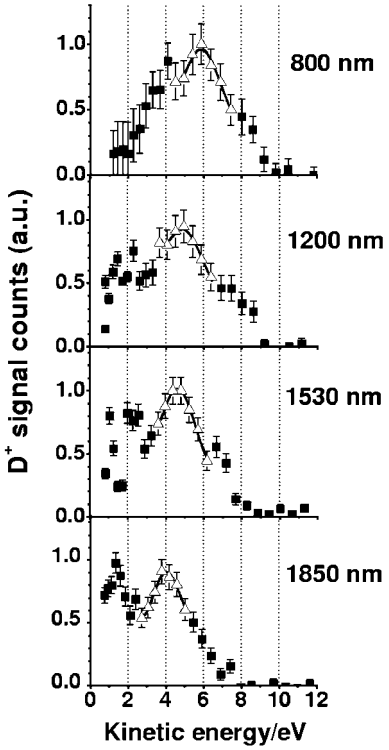

Figure 9. Kinetic energy release spectra for D_2 were recorded for several different laser wavelengths. By changing the wavelength, the time between ionization and recollision was changed. It is apparent that the vibrational wave packet in D_2^+ is moving outwards, since the kinetic energy release is decreasing. The curves are fits to the peaks.

The first experiment to utilize the femtosecond-duration recollision electron wave packet as a probe of dynamics was by Niikura *et al* [65]. In conventional pump–probe experiments, the system is excited by a pump pulse, and after a variable delay time the system is interrogated by a probe pulse. Clearly, both the pump and probe pulse durations must be shorter than the time scale of the dynamics being investigated.

Instead, Niikura used a laser pulse that lasted much longer than the dynamics. He relied on the time delay between the ionization of the system and the returning electron to give the pump–probe delay. He studied vibrational motion in D_2^+. At some optical cycle within the 40 fs laser pulse, near the peak of the cycle, an electron was tunnel-ionized from the neutral D_2 molecule. This initiated motion on the Σ_g surface of D_2^+, just as in the molecular clock experiment. After about 1/3 of an optical cycle, the electron returned to the parent ion, and could excite the ion. This again led to dissociation, and the kinetic energy of the fragments contained an image of the vibrational wave packet projected onto the Σ_u surface.

But how to vary the pump–probe delay time, when the optical cycle determines the electron's trajectory? By varying the frequency (or wavelength) of the laser. Using an optical parametric amplifier, Niikura recorded the kinetic energy spectra for a range of wavelengths, as shown in figure 9. As the wavelength was increased, and hence as the pump–probe delay time was increased, the kinetic energy release became smaller. Due to the projection onto the Σ_u surface (figure 7), lower kinetic energy corresponds to greater internuclear separation.

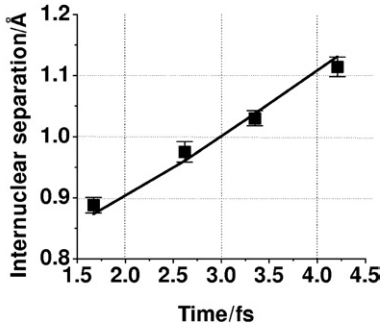

Figure 10. From the kinetic energy peaks of the previous figure, the internuclear separation of D_2^+ is inferred. The time delay is chosen as the time from the peak of the optical field cycle to the centre of the first returning electron wave packet. The velocity of the nuclear vibrational wave packet is self-consistently determined from the slope of the curve, and is solved for iteratively. The line is from a time-dependent Schrödinger calculation of the motion of D_2^+ on the Σ_g surface. The time resolution of this measurement, given as the separation between time points, is less than 1 fs. This demonstrates that a 40 fs, 800 nm laser pulse can give sub-femtosecond time resolution and sub-0.02 Å spatial resolution.

The peaks of figure 9 were fitted with a Gaussian shape to characterize the most probable kinetic energy release. Using the shape of the potential energy surfaces (figure 7), this was translated into a most probable internuclear separation for each pump–probe time delay. This procedure does not take into account the kinetic energy due to the motion of the nuclei themselves. To correct for this, the velocity of the nuclei was determined from the change in the separation as a function of time.

The inferred motion of the vibrational wave packet is shown in figure 10. The nuclei can be seen to be moving apart at each time step. The solid line indicates a time-dependent Schrödinger equation calculation for the wave packet motion on the two surfaces in the laser field. Since the two middle points are separated by less than 1 fs, it can be claimed that this is an attosecond measurement. At the same time, the internuclear separation resolution is better than 0.02 Å. Thus, using a 40 fs laser pulse from an 800 nm wavelength laser, we can achieve resolutions of attoseconds and sub-ångstroms. This is an example of the power of recollision electrons.

3.2. Imaging of molecular orbitals

The process of tunnel ionization followed by recombination leads to the emission of high harmonic radiation. The spectrum and phase of the emitted radiation contain information on the electronic orbital that is ionized. In the case of a molecule, which has a spatial structure that can be oriented, the shape of the highest occupied molecular orbital (HOMO) can be imaged in three dimensions under certain circumstances.

Techniques have been developed in the last few years to align gas-phase molecules using laser pulses. Adiabatic alignment is achieved using aligning pulses that are long relative to the rotational time scales of the molecule of interest, typically hundreds of picoseconds [68–71]. Molecules can be aligned in 3D [72] or oriented if they have a dipole moment [73].

An experimentally simpler technique can be used to align molecules using a femtosecond laser pulse, called impulsive alignment [74]. A 100 fs pulse of non-ionizing intensity applies an angular impulse to the molecules that depends on their orientation relative to the laser polarization axis. This produces a superposition of rotational eigenstates that evolve in phase

after the laser pulse has disappeared. Periodical rephasings of the rotational wave packet result in brief periods when the molecules come into alignment. The advantage of this technique is that the alignment occurs in the absence of the laser field, i.e., field-free. It is then just a matter of delaying the probe pulse for a few picoseconds for it to interact with an aligned sample of molecules.

Above, we have estimated the temporal amplitude and spectral phase of the wave packet. Here, however, we will make no assumptions about the returning electron wave packet and instead describe it as an expansion of plane waves. In particular, we will assume that they are plane waves travelling parallel to the laser field, although that assumption is not necessary. When restricted to polarization direction x, equation (8) can be written in the form

$$\psi_c(x) = \int \mathrm{d}k\, a_k\, \mathrm{e}^{\mathrm{i}kx}. \tag{14}$$

Phase and spectral amplitude of the wave packet a_k are given by equations (9) and (10).

The signal emitted by a single atom is obtained from the second derivative of the dipole equation (11) resulting in the spectral amplitude

$$S(\omega) = \omega^4 |a_k \langle 0|x|k\rangle|^2. \tag{15}$$

Here, $|k\rangle$ is a plane wave of momentum $k = \sqrt{2(\omega - I_p)}$ and $\langle 0|$ is the ground electronic state that has been ionized.

We do not need to evaluate the coefficients a_k. Instead, we use a reference atom whose orbital shape we know. In order to assure that the returning electron wave packet is the same for both, the reference atom and the molecule to be studied, we choose an atom whose ionization potential is very close to that of the molecule. This ensures that they ionize at the same laser intensity. Then the transition dipole moment of the unknown molecular orbital is given in terms of the known reference atom's,

$$|\langle 0; \theta|x|k\rangle| = (S(\omega; \theta)/S_{\mathrm{ref}}(\omega))^{1/2} |\langle 0_{\mathrm{ref}}|x|k\rangle|. \tag{16}$$

Here it is assumed that the rescattering wave packets do not depend on the structure of the parent atom or molecule. This is true to a large extent because the tunnel through which the electron wave packet must escape the parent molecule acts as a spatial filter to remove details of the original wavefunction. In the case of molecules with a π orbital nodal plane, this nodal plane can persist into the continuum. For example, benzene is known to have a node in its continuum electron wave packet [75], as does oxygen. Furthermore, there is an orientation dependence of the ionization rate that contributes to the overall magnitude of the continuum wave packet. This can be calculated, e.g. [24], or it can be measured [76].

The relative phases of the transition dipoles can be separately determined, either by directly measuring the phase of the high harmonic emission [77] or by interfering the two signals from a mixed gas. In this way, the amplitude and phase of the transition dipole moment for an unknown aligned molecular orbital can be determined relative to that of a reference atom. In principle the simplest atom, hydrogen, could serve as the reference.

By changing the relative angle between the polarization axes of the pump (aligning) laser and the probe (ionizing) laser, one can build up a set of projections of the molecular orbital. This can be inverted by using an algorithm based on computed tomography [78], resulting in an image of the molecular orbital. This has been done [3] for di-nitrogen using argon as the reference. Experimental high harmonic spectra were recorded at 19 angles of the molecular axis relative to the laser polarization axis. These spectra were normalized to the recollision electron wave packet complex amplitude versus energy, including the orbital shape of the reference argon atom. The normalized spectra are seen in figure 11. The image in figure 12 shows the $3\sigma_g$ orbital that was unfolded from this set of spectra.

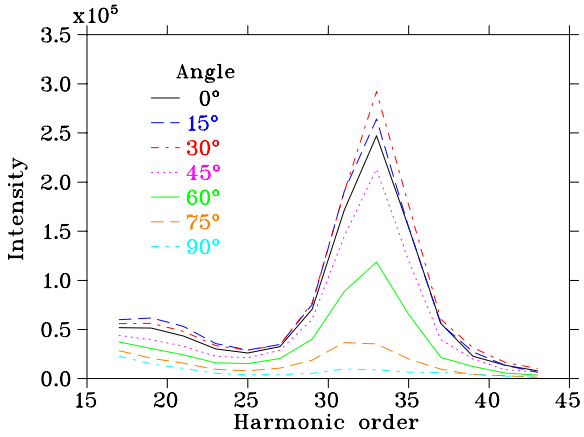

Figure 11. High harmonic spectra were recorded at 19 different angles of the molecular axis relative to the laser polarization direction, only some of which are shown here. The spectra shown have been normalized to the spectrum from the reference argon atom, including the dependence of the transition dipole matrix elements on the orbital shape of the argon $3p_z$ orbital.

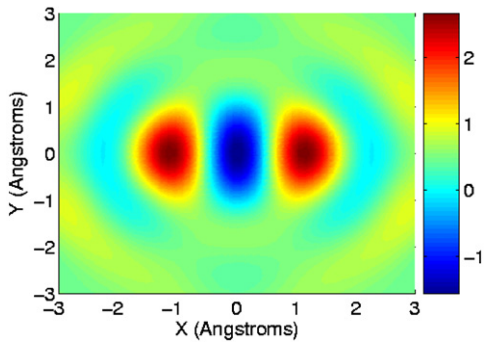

Figure 12. The orbital shape of the $3\sigma_g$ HOMO of N_2 is imaged by recording the high harmonic spectra from N_2 aligned at 19 different angles relative to the laser polarization direction. By applying a tomographic algorithm, the orbital wavefunction shape is determined. Note that this is not the orbital density, but a wavefunction to within a global phase.

The technique of molecular orbital tomography uses laser pulses with durations of 25 fs or less. Molecular dynamics can then be resolved in pump–probe schemes, by observing changes to the orbital structure with time. It can also be extended to observe true attosecond bound state dynamics in atoms [79]. First, an electron wave packet must be excited in the atom, using a short wavelength laser pulse. Then, a few-cycle laser pulse, which is phase locked to the excitation pulse, ionizes the atom. Since tunnel ionization is selective to the highest electronic state, it is the excited state that is ionized. In the semi-classical picture, recombination occurs to both the excited state and the ground state, leading to an interference term. The HHG spectrum will be modulated. The modulation period contains information about the temporal period of the bound state electronic wave packet.

We know that the recollision electronic wave packet is chirped in momentum and that different harmonics are emitted at different times. This maps time onto frequency, much like a streak camera (cf section 2.5). Different spectral components probe different times during the motion of the bound state wave packet. By introducing a time delay between the excitation

and probe pulses, the motion of the bound state electronic wave packet can be mapped out. This offers the first method to observe bound state motion within an atom or molecule.

3.3. Double ionization

Almost all of strong field physics makes the assumption that only one electron is involved in the interaction of the laser field with the atom or molecule. All other electrons are assumed to be passive spectators. This is the single active electron approximation and is generally a good one.

There is a number of observations in strong field physics that are clearly two-electron effects. Double ionization of atoms is an example. When double ionization was first seen, it was realized that it was occurring at a rate much too high to be explained by a sequential process, where first the atom is singly ionized and a second electron is removed from the ionic ground state. One of the first attempts to explain the results was to invoke a process that is well known in XUV inner-shell photoionization—shake-up or shake-off.

Shake-up is the process by which the outgoing photo-detached electron collides with another electron on its way out, thereby causing an excitation. In the presence of a strong laser field, this excited state is likely to field-ionize. Shake-off is the same process that results in an immediate double ionization.

Since that time, it has become apparent that enhanced double ionization of atoms can be explained by the recollision model. However, it is only recently that an estimate of the contribution of shake-up to double ionization has been made [80].

In that experiment, the molecular clock is used as a timer to look for two ionization events that occur within a short period of time of each other. Deuterium is used as the clock. A 40 fs circularly polarized laser pulse induces ionization in D_2. This immediately launches a vibrational wave packet in D_2^+. If shake-up were to occur, it is most likely to be to the first excited state, Σ_u. The excited molecular ion will then field-ionize, at the latest when the internuclear separation reaches the enhanced ionization region.

In order to find a weak signal among many single ionization events, the experiment was designed to look for coincident deuterons. Only shake-up events could produce correlated fragments of high kinetic energy, because the molecular ion would be promoted early to the dissociative state (figure 7). The kinetic energy release spectra are shown in figure 13. The events with energy greater than 8 eV are taken to be due to almost instantaneous double ionization by shake-up. The experiment established an upper limit to the shake-up branching ratio of 10^{-6} at 3×10^{14} W cm^{-2} and 2×10^{-5} at 10^{15} W cm^{-2}. Therefore it is safe to say that excitation of atoms and small molecules is relatively unlikely at these intensities. Excitation may be more significant for larger molecules, in which the excited states are lower lying.

A recent experiment to study the double ionization of neon revealed evidence of sub-femtosecond electron correlations [16]. The apparatus was a COLTRIMS machine (cold target recoil ion mass spectrometry) [81], in which the three-dimensional velocities of electrons and ions could be measured. The device included a cooled supersonic nozzle from which the gas of neon was emitted. The laser beam was focused at right angles to the atomic beam. Ions produced by the laser pulse were accelerated by an electric field to a delay-line anode imaging microchannel plate. At the same time, electrons were accelerated in the opposite direction to a second detector. The electrons were also guided by a magnetic field. Since the detectors could register both the position and time of each event, it is possible to determine the three-dimensional momentum of each particle.

The laser was based on a Coherent RegA regenerative amplifier system. This laser is pumped by a continuous laser source, so that its repetition rate is limited only by the

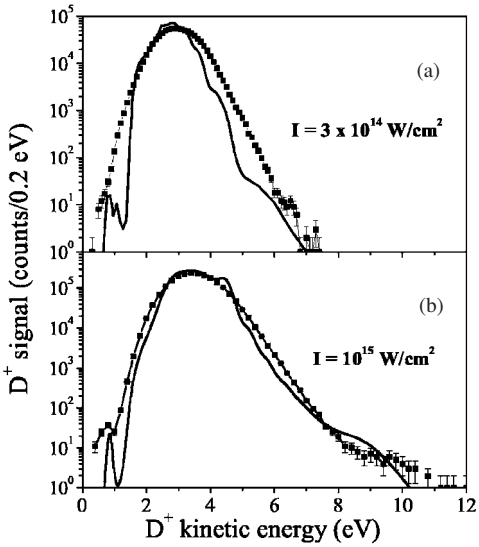

Figure 13. Kinetic energy release per D^+ fragment is a measure of the time delay between ionization and second ionization. Those fragments with greater than 8 eV are due to almost simultaneous double ionization due to shake-up processes. There is no evidence for shake-up at the lower intensity and at 10^{15} W cm^{-2} the branching ratio is 2×10^{-5}.

gain lifetime of the Ti:sapphire laser medium. Repetition rates up to 250 kHz are possible, although 30 kHz was used due to limitations in the detection electronics. This high repetition rate was invaluable because many more events could be recorded compared with a kilohertz laser system. The pulse energy was only 4 μJ per pulse, and was focused with an on-axis parabolic mirror, achieving intensities of 2×10^{14} W cm^{-2}. Pulse duration was 40 fs at 800 nm wavelength.

The laser intensity corresponds to a ponderomotive energy $U_p = 11$ eV. The maximum kinetic energy of an electron as it returns to the parent ion is about 41 eV. The ionization potential of the neon ion, Ne^+, is 41 eV. The lowest excited state of Ne^+ is 27 eV. Thus the returning electron will have sufficient energy to excite the ion, but not to remove another electron directly.

The momentum of each electron in double ionization events was recorded. Figure 14(a) shows the two-electron momentum correlation in the plane parallel to the laser electric field axis. It can be seen that the electrons are preferentially emitted in the same direction.

Figure 14(b) shows the perpendicular momentum correlation for those electrons that were emitted in the same direction, labelled as regions A in the top panel. The first electron's momentum was rotated so that it pointed up in the graph, and the distribution shows the relative momentum of the second electron. The distribution can be seen to be about 0.1 au below the origin, indicative of repulsion. In contrast, panel (c) shows that electron pairs from regions B do not show repulsion.

What does this tell us about the time at which the electrons are liberated? Panel (a) tells us that the two electrons are freed during the same optical half-cycle, i.e., within about 1.3 fs of each other. Panel (b) shows that the two electrons feel each other's electric field, and repel each other. Both electrons must squeeze through the tunnel produced by the laser field and the ion's potential in less than 1 fs. The actual time difference can be modelled to estimate the average time difference between each electron emerging from this tunnel. The conclusion of

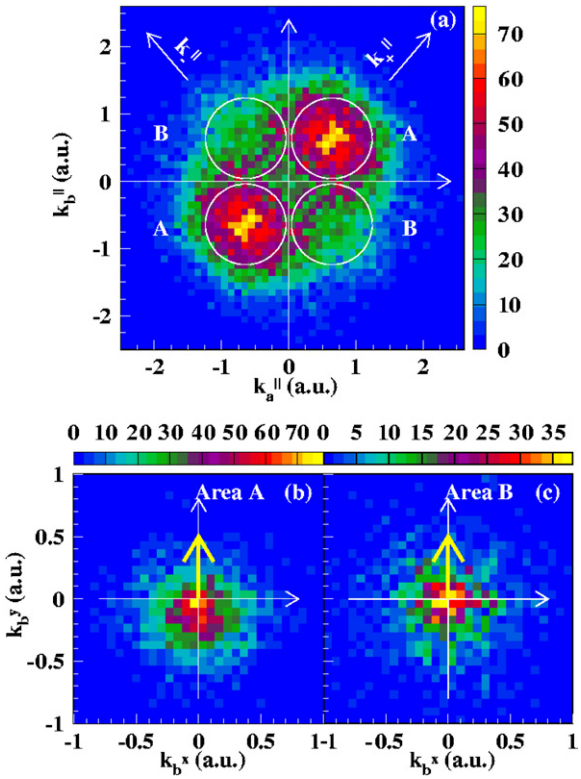

Figure 14. Results of double ionization of Ne using an 800 nm laser with intensity of 1.9×10^{14} W cm^{-2}. Panel (a) shows the relationship between each electron's momentum component parallel to the laser polarization direction. Events in quadrants labelled A mean that both electrons are detected going in the same direction. It can be seen that most electron pairs do travel in the same direction. Panel (b) shows the momenta in the plane perpendicular to the laser polarization corresponding to those events only from quadrants A. The first electron is defined as going upwards. The distribution is shifted downwards, indicating that the electrons repel each other. In panel (c), with events from quadrants B, there is no such repulsion. This measurement suggests that the two electrons are ionized at almost the same instant.

this work is that the recolliding electron briefly creates a double excited state in Ne, and that both electrons are then ionized by the field at about the same time.

4. Attosecond pulses

The high harmonic radiation generated by an intense laser pulse passing through a dilute gas has an attosecond time structure. These pulses have been used in a variety of experiments first to measure properties of the XUV pulse itself, to produce an image of the laser pulse, to generate ultra-short electron wave packets and to time-resolve an Auger relaxation process. In all these experiments the XUV pulse was cross-correlated with the generating laser pulse.

4.1. Trains of attosecond pulses

The first unambiguous measurement of attosecond structures in the harmonic radiation generated by a multi-cycle laser pulse [82] was based on laser-dressed photoionization by

the harmonic radiation. As explained in section 2.3, harmonic radiation generated by a long pulse has clearly defined peaks at odd multiples of the fundamental frequencies. The harmonic field can be written as

$$\mathcal{E}_h(t) = \mathrm{Re}\sum_{n=0}^{\infty} \exp(\mathrm{i}(2n+1)\omega t + \varphi_{2n+1})|a_{2n+1}|, \tag{17}$$

where the power spectrum $|a_{2n+1}|^2$ is measured directly. Linear dependence of the phases φ_{2n+1} on n translates into a time shift $t \to t + \Delta t$. The time structure is determined by the second phase differences $\delta^2\varphi_n = 2\varphi_{2n+1} - \varphi_{2n-1} - \varphi_{2n+3}$.

Photoionization by the harmonic radiation produces a sequence of photoelectron energy peaks that are separated by twice the laser photon energy. When one dresses photoionization by the generating laser field, a two-photon (laser plus XUV) process produces sidebands between the photoelectron peaks. The intensity of the side-bands beats with the relative delay between harmonic and laser pulses at twice the laser frequency. The beating is due to the interference of two alternate paths leading to the same side-band peak, adding one laser photon to a harmonic photon $(2n-1)\omega + \omega$ or subtracting one laser photon from the next higher harmonic photon $(2n+1)\omega - \omega$. It was found in [83] that there is a phase difference between the beats of subsequent side-bands, which is equal to the second difference $\delta^2\varphi_n$ of the relative phases of the three nearest harmonic peaks (up to a well-known phase due to the XUV ionization process).

In [82] the laser and the harmonic pulse train were cross-correlated in an Ar gas jet. The observed side-band beats allowed us to determine the phase shifts between subsequent harmonics, from which a duration of 250 as for the individual peaks of the XUV pulse train was deduced.

4.2. Single attosecond pulses

4.2.1. Phase-stabilized few-cycle pulses. As discussed in section 2.3, few-cycle laser pulses with well-defined carrier–envelope phase are a prerequisite for generating single, isolated attosecond XUV pulses. While there are several different methods of generating phase-stabilized laser pulses, e.g., in OPAs [13], a very straightforward method can be used to upgrade existing oscillator and amplifier laser systems [8, 84–88] as follows. Because of the difference between phase and group velocity, the carrier–envelope phase of subsequent pulses from an oscillator with repetition frequency ω_{rep} drifts from shot to shot by

$$\Delta\varphi_{\mathrm{CE}} = 2\pi\,\omega_{\mathrm{CE}}/\omega_{\mathrm{rep}}. \tag{18}$$

To measure ω_{CE} one generates the second harmonic of an octave-spanning frequency comb spectrum and brings the low frequency modes of this spectrum in interference with the high frequency modes of the fundamental. The resulting signal beats at carrier–envelope frequency: $\omega_{\mathrm{CE}} = 2(n\omega_{\mathrm{rep}} + \omega_{\mathrm{CE}}) - (2n\omega_{\mathrm{rep}} + \omega_{\mathrm{CE}})$ [89]. As an octave-spanning spectrum is not available from a typical mode-locked oscillator or a chirped-pulse amplifier, a medium with a third-order nonlinearity has to be employed for white-light generation. For nJ pulses a photonic crystal fibre can be used, whereas for amplified pulses a split-off of less than 1% can be sufficient for white-light generation in a sapphire plate. The output of this 'f-to-2f interferometer' (figure 15) can be used for a feedback loop to stabilize the carrier–envelope phase [84]. For an amplifier system one employs one feedback loop for the oscillator and a second loop which addresses the same actuator (e.g., an acousto-optic modulator in the oscillator pump beam) to pre-compensate for the slow phase drift introduced in the amplifier [13].

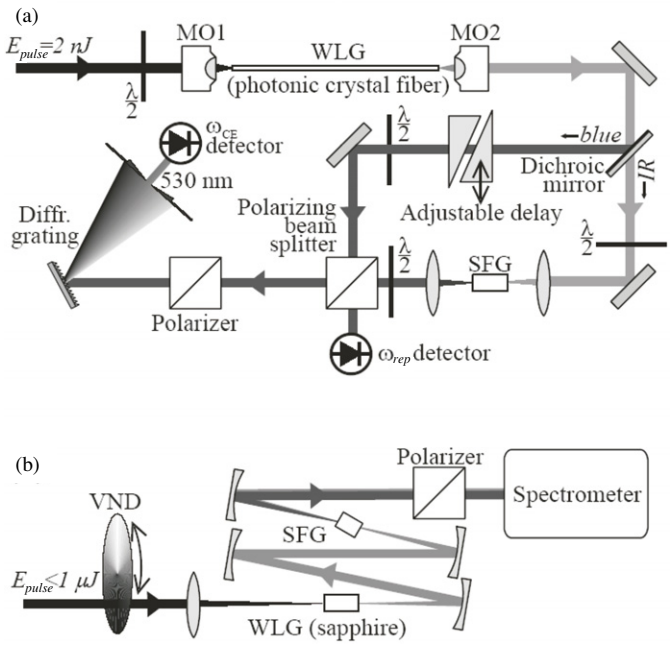

Figure 15. Schemes for measurement of CE phase drift. (a) Nonlinear Mach–Zehnder interferometer for characterization of low energy mode-locked oscillators. (b) Set-up for phase characterization of amplified pulses by nonlinear spectral interferometry. MO1, 2: microscopic objective lenses. VND: variable neutral density filter. SFG: sum frequency generator. WLG: white-light generator. $\lambda/2$: half-wavelength wave plates.

4.2.2. Characterization of single attosecond pulses. Attosecond pulse characterization is based on the streaking method introduced in section 2.5. The experimental realization of this technique falls within a class of experiments that began with the work of Schins and co-workers [90–94]. Here, the XUV pulse is 'cross-correlated' against a short visible pulse. An XUV photon excites a bound atomic electron into a positive-energy state in the presence of a laser field. Laser-induced transitions from this state or a laser-induced shift in its energy (Stark shift) provide the nonlinearity linking the XUV to the laser pulse. The spectral width of XUV pulses that can be analysed by these methods is limited by the laser photon energy to $\lesssim$2 eV, as laser generated side-bands must be distinguishable.

The streaking method avoids this difficulty, as the cross-correlation is with the sub-laser-cycle variations of the electric field rather than with the average intensity during a complete laser cycle. As discussed above, the time structure of the XUV pulse is transformed into a modulation of momentum spectra obtained from laser-dressed XUV photoelectron emission.

The experimental set-up for the generation of sub-femtosecond XUV pulses by high harmonic generation (HHG) and attosecond metrology (by laser-assisted XUV photoionization) [4, 46, 62] is displayed in figure 16.

Harmonics are generated in a Ne gas jet. The central part of the laser beam is blocked by a Zr foil that is transparent for the harmonic beam. Cross-correlation between laser and XUV pulses occurs in a second gas jet. The time delay between the co-propagating XUV and laser pulses is controlled by a split mirror, whose inner part is movable in steps of 10 nm, generating time-delay steps of $\sim 2 \times 30$ as. A multi-layer mirror on the movable part filters a maximal bandwidth of $\sim$10 eV around a photon energy of 90 eV. The kinetic energy of

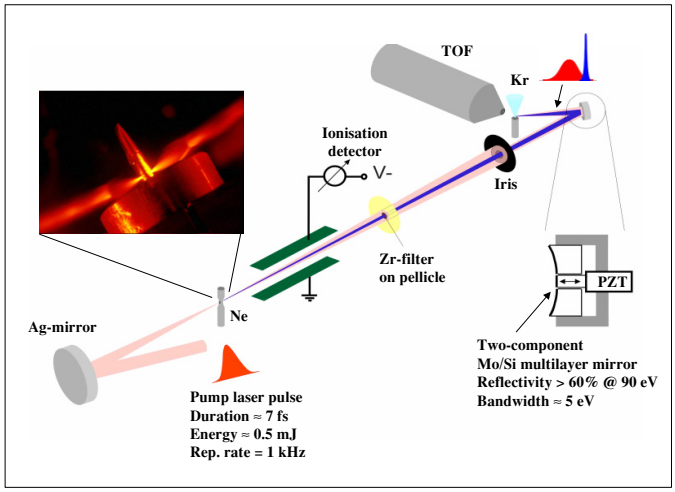

Figure 16. The schematic of the experiment. The focused 7 fs laser beam interacts with neon atoms to produce high harmonic radiation. The laser and the highly collimated XUV beam co-propagate collinearly through a 2 m beam line towards the measurement. In the beam line the laser and harmonic beams pass through a 200 nm thick, 3 mm diameter zirconium foil placed on a 5 μm thick nitrocellulose pellicle to cover a hole of 2 mm diameter. The energy transported by the resulting annular beam can be adjusted with a motorized iris between a fraction of a microjoule and a few tens of microjoules. The Mo/Si multi-layer consists of an annular part having an outer diameter of 10 mm with a concentric hole of 3 mm diameter hosting a miniature mirror of slightly smaller diameter. Both parts originate from the same substrate, ensuring identical radii of curvature ($R = 70$ mm). The miniature central mirror is mounted on a wide range, nanometer precision piezo-stage, allowing alignment and translation with respect to the external part.

the photoelectrons is determined from their time-of-flight distribution measured with a micro-sphere plate detector and a multi-channel analyser. Integrating over 40 000 shots gives good enough statistics for evaluatable spectra. With this apparatus single pulses as short as 250 as have been measured [4].

4.3. Time-resolved measurement of an Auger decay

Pump/probe experiments are the most direct approach to tracing fast dynamics in the time domain. The extension of time-resolved (pump–probe) spectroscopy to ultrafast electronic processes taking place deep inside atoms has so far been frustrated by the simultaneous requirements of short wavelengths (i.e., high photon energy) and sub-femtosecond pulse duration. In addition, for a straightforward interpretation of spectroscopic data *isolated single* pulses [95, 96] were needed. With single attosecond pulses and a precisely timed laser pulse, the streak-camera concept can be extended for sampling the emission of secondary (Auger) electrons. In that way, one can time-resolve an atomic inner-shell process with attosecond accuracy.

The principle of the measurement is illustrated in figure 17. The sub-femtosecond XUV pulse excites a core electron and produces a short-lived inner-shell vacancy. This is rapidly filled by an electron from a higher energy level (outer shell). The energy lost by the electron is carried away either by an energetic (XUV/X-ray) photon or by a secondary (Auger) electron. The emission time of this Auger electron corresponds exactly to the lifetime of the inner-shell vacancy. Hence, sampling the Auger electron emission with the oscillating laser field

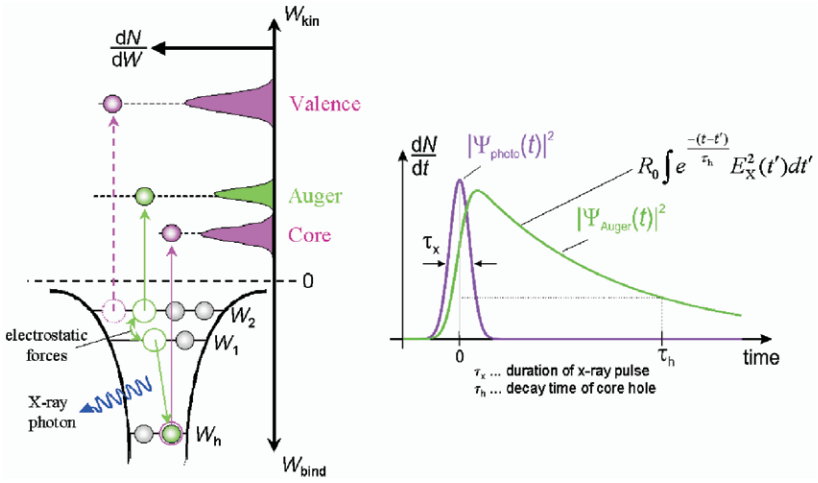

Figure 17. Schematic and temporal evolution of the Auger process.

in the same way as we sampled the photoelectron emission gives us direct time-domain access to inner-shell atomic processes with attosecond resolution. The first proof-of-principle experiment was recently demonstrated [5]. As the decay time measured in this experiment can also be inferred from energy-domain measurements, it served as a benchmark for the new methods of attosecond time-resolved spectroscopy.

5. Future short pulse sources

Attosecond physics so far has relied on pulses from high harmonic generation. The minimum pulse duration from the harmonic process may be as low as 50 as or less when very high intensities are combined with pulse compression schemes [97] or when pulses with time-dependent polarization are used [98]. The major drawback of the harmonic pulses is their intrinsically low intensity due to the close connection between harmonic generation and ionization. Therefore, in addition to the generation of shorter harmonic pulses, we briefly discuss alternative short pulse sources that employ Raman scattering, plasma mirrors, or a combination of two or more phase-locked lasers.

5.1. XUV pulse compression

Harmonics generated by recollision are chirped. For short trajectory harmonics, which are used in most experiments, the chirp is positive, i.e., higher frequencies are generated at later times (cf figure 3). The measured frequency dependence of harmonic emission times [67] fully confirms the theoretical prediction. The positive chirp can be compensated by sending the harmonic beam through a medium with negative dispersion. In [17] an attosecond pulse train was sent through a slab of aluminium, which reduced the duration of the spikes in the pulse train from 450 as to 170 as, which are the shortest measured harmonic pulses at present.

Pulse compression is only effective for harmonics below the cutoff. These harmonics are generated repeatedly and therefore come in pulse trains. The single harmonic pulses produced in the cutoff region were found to be nearly transform limited and cannot be compressed by means of linear optics. Recently, it was proposed to generate *single* harmonic pulses from

harmonic radiation generated below the recollision cutoff energy [97]. The idea is to use a short and very strong laser pulse, such that the medium is completely ionized during a single laser half-cycle in the rising flank of the pulse. A single burst of high frequency radiation is generated with a broad spectrum and nearly linear chirp, but all further bursts after that are suppressed because of the destruction of the atom. If the chirp can be compensated by a suitable material pulses as short as 50 as result. For this scheme, pulse intensities and the atomic species must be carefully selected in order to avoid harmonic generation from multiple ionization.

5.2. Single-cycle pulses in the visible and UV from molecular modulators

Searching for efficient nonlinearities which can lead to nearly complete conversion of the incident energy into new radiation, one inevitably comes across Raman scattering.

High-order stimulated Raman scattering has long been known to lead to very efficient conversion of incident radiation into Raman side-bands. Early theoretical studies of the propagation of intense femtosecond pulses in a Raman-active medium include predictions of attosecond pulse generation [99–101]. Reference [102] (see also [103]) suggested the use of multi-component Raman spectra for femtosecond time scale pulses. References [104–107] demonstrated extremely broad spectra with discrete lines from the far IR to the extreme UV, including rotational side-bands from droplets of solid hydrogen [105, 106]. References [108, 109] suggested that high-order Raman scattering can lead to the formation of attosecond Raman solitons.

Recently, several experiments demonstrated very efficient compression of incident near-IR or visible/UV pulses down to one- or two-cycle duration with spectra extending from near-IR to near-UV, with nearly 100% efficiency. The experiments were performed in two completely different interaction regimes. In the first regime, a pair of long pulses is tuned near resonance with the Raman transition [107, 110–112]. The two pulses excite the medium as they propagate along and are modified by the interaction with the medium during propagation. The second regime is the pump–probe regime of impulsive excitation of the Raman medium [113–116]: first a short pulse with spectral bandwidth exceeding the frequency of the Raman transition 'hits' molecules in the medium and leaves Raman excitation in its wake, and then a delayed probe pulse scatters off the prepared excitation in the medium. Significant broadening of the spectrum accompanied by pulse compression has also been observed in this regime in [117–120].

Generation of ultra-short optical pulses involves two major steps. First, new frequency components should be generated. Second, phases of different spectral components should be adjusted (linearized) to obtain a short pulse. A unique aspect of the approach which uses a Raman-active medium is that both steps can occur simultaneously, and the pulse can be compressed automatically during propagation by dispersion, both in the adiabatic [103, 107, 110] and the impulsive [113–115, 121–125] regimes.

In the adiabatic excitation regime, hydrogen and deuterium molecules were used as the Raman-active medium. The observed Raman spectrum spans four octaves or more, extending from 3 μm in the near-infrared to at least 195 nm in the ultraviolet [126], converting nearly 100% of the input energy into the Raman spectrum, and capable of supporting pulses of about 600 as. Using both manual and electronic techniques to control the phases of a small subset of these side-bands, single-cycle 2 fs pulses in the visible were made and measured.

In the impulsive regime, various molecules have been used, including CO_2 and SF_6. The shortest pulses produced were below 4 fs in the near-UV, with central wavelength around 400 nm [115]. The possibility of optimizing the interaction for automatic self-compression of

the probe pulse during propagation in the pump–probe regime has been studied in [121, 122, 124], where it was shown that tunable nearly single-cycle pulses can be produced in a broad frequency range, from mid-IR to UV.

In a mixture of D_2 and H_2, sets of side-bands with incommensurate frequencies will be produced: $\omega_{KN} = \omega + K\omega_{\mathrm{Ram,H}} + N\omega_{\mathrm{Ram,D}}$, where $\omega_{\mathrm{Ram,H}}$ and $\omega_{\mathrm{Ram,D}}$ are the frequencies of either vibrational or rotational excitation of the H_2 and D_2 molecules. Selecting different side-band subsets from multiplicative or additive side-band spectra allows one to engineer very complex waveforms, with single-cycle main pulses separated by long time intervals [126–128].

Let us consider the key physics behind these results. The discussion below draws upon theoretical analysis of side-band generation in [103, 107, 110, 126] for the adiabatic regime and [121–124, 129] in the pump–probe (not necessarily impulsive) regime.

Let us start with the adiabatic regime. In [103, 107, 110–112], two ns pulses are detuned in frequency by $\Omega \approx \omega_{\mathrm{Ram}}$, where ω_{Ram} is the frequency of either vibrational or rotational excitation of the molecule. The pulses are sent collinearly into a cell of molecules H_2 (and/or D_2) at liquid nitrogen temperature. The molecules only react to the intensity beat between the two close frequencies, as the carrier oscillations are too fast. For the sake of argument, let us assume that the Raman excitation is tuned to vibrations in H_2. The intensity beat forces the molecules to vibrate, stretching and compressing periodically. If the beat frequency is slightly lower than the vibrational frequency, the molecule will be forced to vibrate in phase with the intensity beat: high intensity will coincide with maximal stretch of the molecular bond. If the beat frequency is slightly higher than the vibrational frequency, the molecule will vibrate out of phase: high intensity will coincide with maximal compression of the molecular bond. As the molecule contracts, its polarizability decreases and so does the refractive index in the medium. As the molecule stretches, the refractive index increases. Thus, incident pulses ride oscillating refractive index $n(t)$.

Propagation in the medium with a time-dependent refractive index shifts the frequency of the laser field. In the simplest zero-order picture, propagation of the wave $\sin(\omega t - kx)$, $k = n\omega/c$ over the length L introduces a *time-dependent* phase shift $\Delta\phi(t) \sim -n(t)\omega L/c$. This implies a frequency shift $\delta\omega \sim -\dot{n}(t)\omega L/c$. In a medium with periodic modulation of $n(t)$, say $n(t) = n_0 + \Delta n \sin\Omega t$, the derivative takes both positive and negative values, broadening the pulse.

Turning to automatic pulse compression in the Raman medium, consider the regime where the maxima in the beat pulse propagate above the minima in the refractive index $n(t)$. The part of the beat pulse arriving just before the minimum, i.e., at earlier times, experiences negative $\dot{n}(t)$ and hence positive frequency shift. The part of the pulse propagating over the minimum in $n(t)$ experiences no frequency shift. The tail of the pulse sees positive $\dot{n}(t)$ and acquires negative frequency shift. As a result, the front of the beat pulse will have higher frequency than its tail. In a medium with normal dispersion higher frequencies propagate slower, allowing the tail of the pulse to catch up, automatically compressing the pulse.

In the pump–probe regime, the physics is similar, but the preparation of $n(t)$ by the pump is decoupled from the compression of the probe. This allows one to tune the medium excitation, the timing and the chirp of the probe pulse to optimize the compression [121, 122, 124].

5.3. The plasma mirror

At present, generation of attosecond pulses via HHG with an atomic gas as nonlinear medium has one significant drawback—the conversion efficiency of the incident radiation

into harmonics is very low. Despite numerous attempts to optimize the process using phase matching in hollow fibres [130], or improving phase matching by optimizing the focusing geometry of the fundamental beam [131–135] or using a self-guided beam [136], the best conversion efficiencies in VUV today stand around 10^{-5} per harmonic peak. The very nonlinearity used for harmonic generation is intimately related to ionization of the nonlinear medium and hence leads to its destruction whenever pushed too hard.

It is therefore attractive to use nonlinearity in a medium which the strong driving field cannot destroy. A plasma is such a medium where the relativistic nonlinearity can be used for harmonic generation. This mechanism is predicted to give much higher conversion efficiency (per cent to tens of per cent level), as well as shorter pulses than conventional HHG [137–140]. Experimental evidence to support these predictions is still lacking, however.

To begin with, let us consider the simplest one-dimensional (1D) model of a planar plasma mirror and a plane wave hitting the mirror at normal incidence (see, e.g., [141–145]). The discussion below follows [139] and discussions presented to one of the authors (MI) by J Meyer-ter-Vehn and S Gordienko. Light pressure (the Lorentz force) pushes the mirror (electrons in the plasma) back, the Coulomb force tries to restore it. This results in periodic oscillations of the plasma mirror with some law $X(t)$. If the light hits the mirror at some moment t', the extra phase acquired by the reflected wave is $\Delta\Phi = \omega 2X(t')/c$, where ω is the frequency of the incident light. If at the field-free boundary $x = 0$ the incident wave is $\propto \sin\omega t$, then the reflected wave at the same boundary is $\sin\omega(t + 2X(t')/c))$, with the relationship between t and t' given by $t' = t + X(t')/c$. Ultra-relativistic motion of the mirror surface $X(t)$ results in a very large number of harmonics in the Fourier spectrum of $\sin\omega(t+2X(t')/c))$ falling off as $N^{-5/2}$ where $N < N_c$ is the harmonic number and the cutoff is $N_c \sim 4\gamma_{\rm rel}^2$ and $\gamma_{\rm rel} = \max\left[1/\sqrt{1 - \dot{X}^2/c^2}\right]$ is the maximum value of the relativistic factor [139]. In the ultra-relativistic regime of $\mathcal{E}/\omega c \sim 20$ the number of emitted harmonics exceeds 10^3. It is also clear that all sufficiently high harmonics are emitted in a very short time interval when the mirror velocity is close to the speed of light c, i.e., during a fraction of the laser cycle.

Conversion efficiency is determined by reflection efficiency; full reflection means that all incident light is converted into the train of ultra-short pulses.

High intensity of the driving field required by the ultra-relativistic interaction regime means that in practice the laser field has to be tightly focused. The limit is the so-called λ^3 regime, where a single-cycle pulse is focused down to the wavelength [137, 138, 140]. Tight focusing conditions add important new physics to the simplified picture above. In a focus, the incident pulse has components normal to the surface that fall onto the plasma boundary at oblique angles and the electric field of the incident pulse has normal component to the surface. If the intensity of the laser light is not too high, these components play an important role. They lead to asymmetry in the laser-induced motion of the plasma, which develops a complicated anisotropic surface structure [140]. As a result, attosecond pulses are reflected at various angles, in specular and non-specular directions. These pulses also have a highly asymmetric structure of carrier oscillations under the envelope and look like half-cycle pulses—but in the XUV rather than THz domain [137, 140].

This physical picture appears as a result of particle-in-cell simulations, and its main features can be summarized as follows [140]. (i) The λ^3 regime reduces instabilities. (ii) A tight focus produces strong alternating slopes in the plasma density, deflecting subsequent half-cycles in different directions and favouring formation of half-cycle pulses. (iii) Reflections from near-critical density surfaces remain efficient. Simulations show that almost 20% of incident energy can be reflected into a single attosecond pulse. One crucial requirement is

stabilization of the carrier–envelope phase of the incident pulse. Without it, the attosecond pulses will not be reproducible, neither in their intensity nor in the direction of propagation.

5.4. Phase-locking several lasers

An extension of locking φ_{CE} of a single laser is to lock the relative phase of two or more fs lasers. Various experiments can profit from such a set-up, the most prominent of them will be pump–probe experiments, especially when two different wavelengths are used (two-colour experiments). Combining phase-locked lasers with broad overlapping spectra would also provide a highly controllable and very broadband coherent source. The first important step towards this goal is to synchronize the repetition rate of two lasers such that the remaining time jitter is less than the oscillation period of the optical carrier wave. The most common techniques available for synchronization are cross-phase modulation to synchronize passively two mode-locked lasers that share the same intra-cavity medium [146–148] and an all-electronic active stabilization [149, 150] which can be further improved by using an error signal generated by an optical cross-correlation [151].

Apart from the synchronization of the repetition rate, coherent locking of the CEP of two separate fs lasers requires measurement and stabilization of the phase difference between the two optical carrier waves. After the repetition rates have been matched ($\omega_{rep1} = \omega_{rep2}$) the carrier–envelope offset frequencies have to be locked. The condition that both lasers have the same phase drift $\Delta\varphi_{CE1} - \Delta\varphi_{CE2} = 0$ implies that the carrier offset frequencies are equal, too: $\omega_{CE12} = \omega_{CE1} - \omega_{CE2} = 0$. ω_{CE12} can be measured by a heterodyne beat signal between frequency comb components of the two lasers [152–154].

6. Outlook

The imaging and pump–probe techniques described above are being further refined and applied to a larger variety of systems. Apart from that, new variations of the techniques are being investigated in two directions: (i) to improve *spatial* resolution and the amount of geometric information that can be extracted and (ii) to investigate processes on significantly shorter time scales, as for deeply bound electrons or in nuclear physics.

6.1. Laser-induced electron diffraction

There have been substantial efforts towards creating sub-picosecond electron beams so that molecular dynamics can be imaged by looking at the time dependence of the diffraction pattern created by the electron pulse [155, 156]. In typical electron diffraction experiments, the electron kinetic energy is 50 keV to 300 keV, with corresponding de Broglie wavelengths of 0.05 Å to 0.02 Å. With typical bond lengths in the range of 1 Å, there will be a number of diffraction orders, making spatial reconstruction simpler and more accurate. The main limitation is that electron pulses will disperse, even in vacuum, due to their mutual repulsion and velocity dispersion. As a result, the time resolution in such diffraction experiments is a few hundred femtoseconds to a picosecond.

Intense laser pulses can also generate a diffraction image of a molecule by recollision with the molecule's own electrons [14, 157–161], with about 1 Å spatial and nearly 1 fs temporal resolution. The basic conditions for the recollision were introduced in section 2.2. Elastic scattering then takes the diffraction image of the parent molecule (figure 18).

From the ion's perspective, during the recollision the electron current density exceeds 10^{10} A cm^{-2} and is concentrated within a small fraction of the laser cycle (<1 fs) [14], exceeding the characteristics of conventional approaches to ultrafast electron diffraction

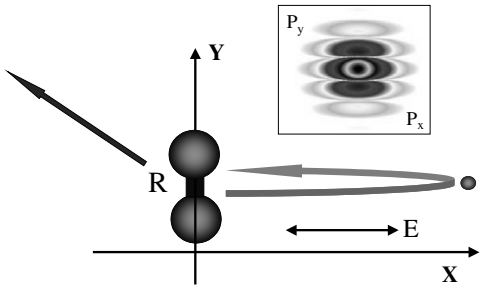

Figure 18. Qualitative idea behind laser-induced electron diffraction imaging: laser field induced recollision between a freed electron and the parent molecular ion. The inset shows the initial electronic state in momentum space with its characteristic diffraction-like structure: the recolliding wave packet carries the imprint of the initial state already prior to the recollision.

by many orders of magnitude. A laser pulse can also be used to align molecules [162], emphasizing the diffraction pattern.

However, the kinetic energy of the electrons is considerably less than is desirable. The maximum kinetic energy of the returning electron is $3.17U_p$ (see section 2.3). At intensity 5×10^{14} W cm^{-2} and wavelength of 800 nm it is just under 100 eV, with a de Broglie wavelength of only 1.3 Å, barely sufficient for resolving a single diffraction order. This problem can be ameliorated by using a long wavelength laser, since the de Broglie wavelength scales as λ^{-1}. Intensity cannot be increased indefinitely—it is limited by multiple ionization of a molecule. Still, it can be increased somewhat by going to nearly single-cycle pulses.

Advantages of laser-induced electron diffraction in terms of time resolution do not come for free: the nature of the electron pulse and the presence of the strong laser field lead to several interesting effects, each of which requires careful consideration.

First of all, the electronic wave packet carries (through the pre-exponential factors) the *imprint of the initial state* (cf section 2.1 and figure 18, inset). Tunnelling ionization allows one to minimize these original structures by imposing an effective Gaussian filter [32–35]. For large molecules, where the electron can emerge from any one of many atoms, such minimization can be very useful. Further, the typical recollision energies in $\lambda = 800$ nm light are ∼100–150 eV. Deflection with relevant transverse velocities $v_\perp \sim \pi/R$ corresponds to *large scattering angles* θ. Quickly decreasing cross sections $d\sigma(\theta)$ distort the diffraction image and weaken the signal. The problem can be remedied by increasing the wavelength of the laser radiation, since recollision energy scales with λ^2. Thirdly, the laser field induces distortions after scattering by further accelerating or decelerating the electron ('post-acceleration'). This clearly affects only velocities in the polarization direction. Therefore, for given recollision energy, the electron's final energy after 'elastic' scattering depends on the deflection angle: the angle-resolved spectrum for a fixed energy does not correspond to a fixed scattering energy. The latter effect can be corrected for by taking proper cuts through the energy and angle-resolved electron spectra [161].

Another effect is interference between diffraction images taken at different energies. Recollision energies vary in time between 0 and $\sim 3.17U_p$. In the absence of the laser field energy-resolved spectra would allow one to discriminate between the diffraction images taken at different energies. However, in the presence of a laser field, electrons recolliding with different energies at different times may end up with the same final velocity due to post-acceleration. The effect is similar to the interference between long and short trajectories, well known in high harmonic generation.

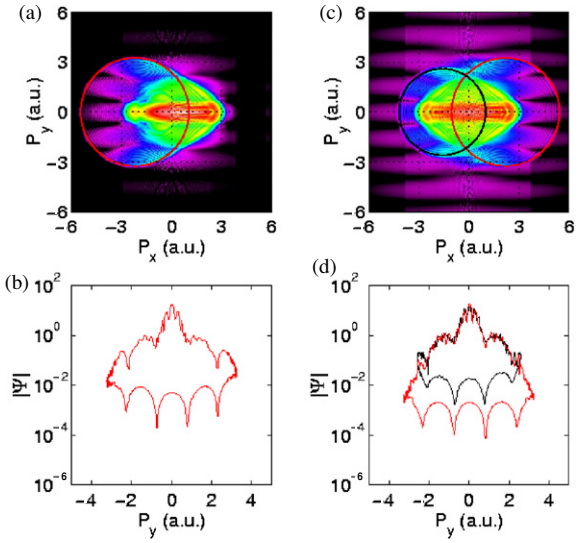

Figure 19. The results of a time-dependent Schrödinger calculation are shown in 2D momentum space. (a) Electron spectrum $|\psi(v_x, v_y)|$ for a 1.25 cycle laser pulse, $I = 6 \times 10^{14}$ W cm^{-2} and $\lambda = 800$ nm. (b) A spectral cut for a fixed moment of recollision, $\omega_0 t \approx 4.4$. (c) and (d) The same as (a) and (b) except they are for a 5 fs duration pulse.

A different type of interference occurs between *multiple ionization and rescattering events*. In a longer laser pulse, the same electron wave packet may return to the ion several times (cf figure 6) and each laser cycle produces a new wave packet. Diffraction images from each recollision interfere, making interpretation of the diffraction patterns even more complicated. As in the case of XUV pulse trains versus single XUV pulses, these problems disappear, when a very short (ideally single cycle) laser pulse is used [160, 161]. One particularly interesting configuration [163, 164], which also eliminates interference of long and short trajectories, is to use two counter-rotating, circularly polarized single-cycle laser pulses with frequencies ω and 2ω. This ensures a single return only, and should make the diffraction images much simpler.

In spite of these complications, one can demonstrate that, under suitable conditions, a diffraction pattern of a diatomic molecule is observed. Spanner *et al* [161] have studied the problem both numerically and analytically. They show that, in the case of a 5 fs laser pulse with a wavelength of 800 nm, it is possible to observe a diffraction pattern from an aligned diatomic molecule when proper directions and energies are selected (figure 19). In addition, they observed a holographic-type pattern that resulted from the interference of the diffracted electron wave with the 'reference' that avoided the molecule. It may be possible to use this pattern to learn about the molecular structure.

The real power of this technique may not lie in determining the molecular structure, but in its sub-femtosecond resolution. Because with a very short laser pulse the individual half-cycle electron pulses can be resolved, the temporal resolution might be as good as half an optical cycle.

6.2. Time-resolving the ionization process

The pump–probe method of [5] is currently being extended to other systems. The first process to study is the dynamics of strong field laser ionization itself. Here the laser, rather than serving as a weak probe, causes strong ionization. An XUV pulse is used to monitor the

depletion of the neutral state and the restructuring of the bound state spectrum from neutral to the ion with sub-laser-cycle time resolution.

A primary goal of the experiment is to observe the depletion of the atomic ground state by the laser field. In the quasi-static picture (cf equation (2)) ionization is expected to be strongly modulated during the laser cycle with rapid decreases of the ground state population near field peaks and constant population near the nodes. The signature of *dynamics* in the proper sense is deviations from the quasi-static picture. A detailed analysis shows that excited bound state dynamics as well as adiabatic distortions of the ground state by the strong field cause deviations from the quasi-static picture [165]. First experiments were performed using Xe gas, as it ionizes at lower laser intensities. While significant sub-laser-cycle time structures were found, their interpretation remains difficult due to the many electrons in the Xe atom. With He the interpretation is expected to be simpler, but a variety of theoretical and experimental questions need to be resolved. High quality vacuum is required to suppress background ionization at laser intensities 5×10^{14} W cm^{-2}. First of all, in this type of measurement laser streaking of the XUV electrons leads to a severe distortion of the spectra. To retrieve spectral information reliable theoretical understanding of the streaking process beyond the strong field approximation is needed. Further, a single-electron picture of the ionization process is very likely inadequate, both because the second electron contributes to the ionization yield and because of electron correlation. Spectral information may help to distinguish the origin of photoelectrons but correlation must be considered as a separate dynamic process on the attosecond time scale. This was pointed out in a recent calculation, where the dependence of single-electron two-photon ionization peaks of helium on pulse duration was studied: 'correlation times' in the range of 1 fs were found [166], consistent with recent experimental results [15].

6.3. Time-resolved nuclear physics

Recollision measurements may be extended to much higher energies and shorter time scales by using very high intensity lasers. Since at intensities around 10^{18} W cm^{-2} electrons are accelerated to near the velocity of light, Lorentz forces become comparable to the electric forces exerted on an electron. The resulting acceleration of the electron in the propagation direction suppresses recollision. It was pointed out that in circular polarization and with a second counter-propagating beam recollision can be recovered [167]. In that configuration the magnetic field remains parallel to the electric field and, instead of suppressing recollision, magnetic trapping enhances recollision currents. Classical trajectory simulations (cf section 3.1) show that current densities may be as large as 10^{10} A cm^{-2}, electron energies may reach into the 10 MeV range, and pulse durations down to 100 as may be reached. It was reported that by exploiting correlations between the electron pulse and the laser field, time resolution may be pushed to near 1 as [167]. This may allow the direct observation of many-body relaxation processes, dissipation and viscosity in nuclei.

6.4. XUV-pump–XUV-probe

Nonlinear optics experiments in the XUV range are exceedingly difficult due to extremely small two-photon cross sections. To date, the only successful autocorrelation measurement using attosecond XUV pulses exploited a specific range of relatively long harmonic wavelength for the two-photon ionization of He [168]. The method in principle is limited to photon energies below the ionization potential of the chosen atomic species. An autocorrelation measurement that is not subject to this limitation was reported recently [169]. Purely XUV pump–probe

experiments, which can be considered a special class of nonlinear optics measurements, cannot be performed with present XUV intensities. This is one of the motivations in the quest for more intense short pulse sources. Once such pulses become available, a new stage of attosecond physics is reached and the whole range of methods of pump–probe technology becomes available. In particular, specific inner-shell excitations might be addressed and perturbations of the system by the probing field could be greatly reduced. It might allow, for example, to monitor the evolution of the electronic wavefunction in photochemical reactions near a conical intersection, where the Born–Oppenheimer picture breaks down.

7. Conclusions

Only five years ago, full control over the light field, control of light–matter interaction on a sub-laser-cycle time scale, attosecond pulses, or the time-resolved observation of valence electron dynamics were put forward as (long term!) goals of the development of few-cycle laser pulses [9]. Now, with all those goals achieved, a large variety of applications is being developed. Time-resolved observations on several different levels have been realized, are being prepared for experiments, or are being intensively studied theoretically. Several of the experiments and techniques were introduced in this review: extremely rapid nuclear motion, the evolution of electronic valence orbitals, and the dynamics of electronic relaxation are being observed with sub-fs and sub-ångstrom resolution. The continued development of experimental possibilities is likely to inspire many more techniques of time-resolved imaging on the molecular, atomic, or even nuclear scale. Nuclear and atomic physicists are challenged to reconsider many processes that have been extensively studied by classical spectroscopic methods in a time-domain setting. The prospect of simultaneously observing nuclear and electronic motion in molecules may make non-Born–Oppenheimer processes like the dynamics at conical intersections accessible to direct observation for the first time. Attosecond physics is becoming a reality.

Acknowledgments

AS and MI acknowledge the support of NSERC SRO grant ‘Controlled electron re-scattering: femtosecond, sub-ångstrom imaging of single molecules’ and AS acknowledges support by the Austria Research Fund (SFB 016). RK acknowledges on APART fellowship from the Austrian Academy of Sciences.

References

[1] Kienberger R *et al* 2002 Steering attosecond electron wave packets with light *Science* **297** 1144
[2] Goulielmakis E *et al* 2004 Direct measurement of light waves *Science* **305** 1267–9
[3] Itatani J, Levesque J, Zeidler D, Niikura H, Pépin H, Kieffer J C, Corkum P B and Villeneuve D M 2004 Tomographic imaging of molecular orbitals *Nature* **432** 867
[4] Kienberger R *et al* 2004 Atomic transient recorder *Nature* **427** 817
[5] Drescher M, Hentschel M, Kienberger R, Uiberacker M, Yakovlev V, Scrinzi A, Westerwalbesloh Th, Kleineberg U, Heinzmann U and Krausz F 2002 Time-resolved atomic inner-shell spectroscopy *Nature* **419** 803
[6] Schenkel B, Biegert J, Keller U, Vozzi C, Nisoli M, Sansone G, Stagira S, DeSilvestri S and Svelto O 2003 Generation of 3.8-fs pulses from adaptive compression of a cascaded hollow fiber supercontinuum *Opt. Lett.* **28** 1987
[7] Steinmeyer G, Sutter D, Gallmann L, Matuschek N and Keller U 1999 Frontiers in ultrashort pulse generation: pushing the limits in linear and nonlinear optics *Science* **286** 1507–12
[8] Ell R *et al* 2001 *Opt. Lett.* **26** 373–5
[9] Brabec T and Krausz F 2000 Intense few-cycle laser fields: frontiers of nonlinear optics *Rev. Mod. Phys.* **72** 545

[10] Baltuška A, Fuji T and Kobayashi T 2002 Visible pulse compression to 4 fs by optical parametric amplification and programmable dispersion control *Opt. Lett.* **27** 306–8

[11] Yamane K, Zhang Z, Oka K, Morita R, Yamashita M and Suguro A 2003 Optical pulse compression to 3.4 fs in the monocycle region by feedback phase compensation *Opt. Lett.* **28** 2258

[12] Kobayashi T and Shirakawa A 2000 Tunable visible and near-infrared pulse generator in a 5 fs regime *Appl. Phys.* B **70** S239–S246

[13] Baltuška A, Uiberacker M, Goulielmakis E, Kienberger R, Yakovlev V, Udem Th, Hänsch T W and Krausz F 2003 Phase-controlled amplification of few-cycle laser pulses *IEEE J. Sel. Top. Quantum Electron.* **9** 972–89

[14] Niikura H, Légaré F, Hasbani R, Bandrauk A D, Ivanov M Yu, Villeneuve D M and Corkum P B 2002 Sub-laser-cycle electron pulses for probing molecular dynamics *Nature* **417** 917

[15] Weckenbrock M, Becker A, Staudte A, Kammer S, Smolarski M, Bhardwaj V R, Rayner D M, Villeneuve D M, Corkum P B and Dörner R 2003 Electron–electron momentum exchange in strong field double ionization *Phys. Rev. Lett.* **91** 123004

[16] Weckenbrock M *et al* 2004 Fully differential rates for femtosecond multiphoton double ionization of neon *Phys. Rev. Lett.* **92** 231002

[17] López-Martens R *et al* 2005 Amplitude and phase control of attosecond light pulses *Phys. Rev. Lett.* **94** 033001

[18] Smirnova O, Yakovlev V S and Ivanov M 2005 Use of electron correlation to make attosecond measurements without attosecond pulses *Phys. Rev. Lett.* **94** 213001

[19] Agostini P and DiMauro L F 2004 The physics of attosecond light pulses *Rep. Prog. Phys.* **67** 813

[20] Scrinzi A, Geissler M and Brabec T 1999 Ionization above the Coulomb barrier *Phys. Rev. Lett.* **83** 706

[21] Keldysh L V 1964 Ionization in the field of a strong electromagnetic wave *Zh. Eksp. Teor. Fiz.* **47** 1945
Keldysh L V 1965 *Sov. Phys.—JETP* **20** 1307 (Engl. transl.)

[22] Landau L D and Lifshitz E M 1977 *Quantum Mechanics: Nonrelativistic Theory* (Oxford: Pergamon)

[23] Ammosov M-V, Delone N-B and Krainov V-P 1986 Tunnel ionization of complex atoms and of atomic ions in an alternating electromagnetic field *Sov. Phys.—JETP* **64** 1191 (Engl. transl.)
Ammosov M-V, Delone N-B and Krainov V-P 1986 *Zh. Eksp. Teor. Fiz.* **91** 2008

[24] Tong X-M, Zhao Z X and Lin C-D 2002 Theory of molecular tunneling ionization *Phys. Rev.* A **66** 033402

[25] Mishima K, Hayashi M, Yi J, Lin S H, Selzle H L and Schlag E W 2002 Theoretical studies of the long-range Coulomb potential effect on photoionization by strong lasers *Phys. Rev.* A **66** 053408

[26] Scrinzi A 2000 Ionization of multielectron atoms by strong static electric fields *Phys. Rev.* A **61** 041402

[27] Milosevic N, Scrinzi A and Brabec T 2002 Numerical characterization of high harmonic attosecond pulses *Phys. Rev. Lett.* **88** 093905

[28] Saenz A 2002 Behavior of molecular hydrogen exposed to strong dc, ac, or low-frequency laser fields. I. bond softening and enhanced ionization *Phys. Rev.* A **66** 063407

[29] Saenz A 2002 Behavior of molecular hydrogen exposed to strong dc, ac, or low-frequency laser fields. II. comparison of *ab initio* and Ammosov–Delone–Krainov rates *Phys. Rev.* A **66** 63408

[30] Nikishov A and Ritus V 1966 *Sov. Phys.—JETP* **23** 168

[31] Delone N B and Krainov V P 1991 Energy and angular electron spectra for the tunnel ionization of atoms by strong low-frequency radiation *J. Opt. Soc. Am.* B **8** 1207

[32] Ivanov M Yu, Smirnova O and Spanner M 2005 Anatomy of strong field ionization *J. Mod. Opt.* **52** 165–84

[33] Goreslavskii S P and Popruzhenko S V 1996 Differential photoelectron distributions in a strong elliptically polarized low-frequency laser field *Zh. Eksp. Teor. Fiz.* **110** 1200

[34] Czirjak A, Kopold R, Becker W, Kleber M and Schleich W P 2000 The Wigner function for tunneling in a uniform static electric field *Opt. Commun.* **179** 29

[35] Goreslavski S P, Paulus G G, Popruzhenko S V and Shvetsov-Shilovski N I 2004 Coulomb asymmetry in above-threshold ionization *Phys. Rev. Lett.* **93** 233002

[36] Paulus G G, Lindner F, Walther H, Baltuska A, Goulielmakis E, Lezius M and Krausz F 2003 Measurement of the phase of few-cycle laser pulses *Phys. Rev. Lett.* **91** 253004

[37] de Bohan A, Antoine L P, Milosevic D B and Piraux B 1998 Phase-dependent harmonic emission with ultrashort laser pulses *Phys. Rev. Lett.* **81** 1837

[38] Baltuška A *et al* 2003 Attosecond control of electronic processes by intense light fields *Nature* **421** 611

[39] Yakovlev V S and Scrinzi A 2003 High harmonic imaging of few-cycle laser pulses *Phys. Rev. Lett.* **91** 153901

[40] Corkum P B, Burnet N H and Ivanov M Y 1994 Subfemtosecond pulses *Opt. Lett.* **19** 1870

[41] Antoine P, Piraux B, Milosevic D-B and Gajda M 1996 Generation of ultrashort pulses of harmonics *Phys. Rev.* A **54** R1761

[42] Taranukhin V D 2004 Attosecond pulse generation by a two-color field *J. Opt. Soc. Am.* B **21** 419

[43] Kitzler M and Lezius M 2005 Spatial control of recollision wave packets with attosecond precision *Phys. Rev. Lett.* to be published

[44] Shan B, Ghimire S and Chang Z 2005 Generation of the attosecond extreme ultraviolet supercontinuum by a polarization gating *J. Mod. Opt.* **52** 277

[45] Balcou P, Salieres P, L'Huillier A and Lewenstein M 1996 Generalized phase-matching conditions for high harmonics: the role of field-gradient forces *Phys. Rev.* A **53** 1725

[46] Drescher M, Hentschel M, Kienberger R, Tempea G, Spielmann Ch, Reider G, Corkum P and Krausz F 2001 X-ray pulses approaching the attosecond frontier *Science* **291** 1923

[47] Yakovlev V S, Bammer F and Scrinzi A 2005 Attosecond streaking measurements *J. Mod. Opt.* **52** 395

[48] Lewenstein M, Balcou P, Ivanov M Y, L'Huillier A and Corkum P B 1994 Theory of high-harmonic generation by low-frequency laser fields *Phys. Rev.* A **49** 2117

[49] Becker W, Lohr A and Kleber M 1995 Light at the end of the tunnel: two- and three-step models in intense-field laser–atom physics *Quantum Semiclass. Opt.* **7** 423–48

[50] Salieres P *et al* 2001 Feynman's path-integral approach for intense-laser–atom interactions *Science* **292** 902

[51] Lewenstein M, Kulander K C, Schafer K J and Bucksbaum P H 1995 Rings in above-threshold ionization: a quasiclassical analysis *Phys. Rev.* A **51** 1495–507

[52] Paulus G G, Grasbon F, Dreischuh A, Walther H, Kopold R and Becker W 2000 Above-threshold ionization by an elliptically polarized field: interplay between electronic quantum trajectories *Phys. Rev. Lett.* **84** 3791

[53] Kopold R, Milosevic D-B and Becker W 2000 Rescattering processes for elliptical polarization: a quantum trajectory analysis *Phys. Rev. Lett.* **84** 3831–4

[54] Kopold R, Becker W, Kleber M and Paulus G G 2002 Channel-closing effects in high-order above-threshold ionization and high-order harmonic *J. Phys. B: At. Mol. Opt. Phys.* **35** 217–32

[55] Bellini M, Lyngøa C, Tozzi A, Gaarde M B, Hänsch T W, L'Huillier A and Wahlström C-G 1998 Temporal coherence of ultrashort high-order harmonic pulses *Phys. Rev. Lett.* **81** 297–300

[56] Balcou P, Dederichs A S, Gaarde M B and L'Huillier A 1999 Quantum-path analysis and phase matching of high-order harmonic generation and high-order frequency mixing processes in strong laser fields *J. Phys. B: At. Mol. Opt. Phys.* **32** 2973–89

[57] Gordienko S and Meyer-ter-Vehn J 2003 Analytic solution of the Schrödinger equation for H-like ions in strong laser fields treating the Coulomb potential exactly: the change of the ionization exponent beyond Keldysh's type theories *Laser Interaction with Matter* ed O N Krokhin, S Y Gus'kov and Y A Merkul'ev *Proc. SPIE* **5228** 416–26

[58] Chirilă C C and Potvliege R M 2005 Low-order above-threshold ionization in intense few-cycle laser pulses *Phys. Rev.* A **71** 021402

[59] Wickenhauser M, Burgdörfer J, Krausz F and Drescher M 2005 Time resolved Fano resonances *Phys. Rev. Lett.* **94** 023002

[60] Zhao Z X and Lin C D 2004 Theory of laser-assisted autoionization by attosecond light pulses Private communication

[61] Itatani J, Quere F, Yudin G L, Ivanov M Yu, Krausz F and Corkum P B 2002 Attosecond streak camera *Phys. Rev. Lett.* **88** 173903

[62] Hentschel M, Kienberger R, Spielmann C, Reider G A, Milosevic N, Brabec T, Corkum P, Heinzmann U, Drescher M and Krausz F 2001 Attosecond metrology *Nature* **414** 509

[63] Mairesse Y and Quere F 2005 Frequency-resolved optical gating for complete reconstruction of attosecond bursts *Phys. Rev.* A **71** 011401

[64] Urbain X, Fabre B, Staicu-Casagrande E M, de Ruette N, Andrianarijaona V M, Jureta J, Posthumus J H, Saenz A, Baldit E and Cornaggia C 2004 Intense-laser-field ionization of molecular hydrogen in the tunneling regime and its effect on the vibrational excitation of H_2^+ *Phys. Rev. Lett.* **92** 163004

[65] Niikura H, Légaré F, Hasbani R, Ivanov M Yu, Villeneuve D M and Corkum P B 2003 Probing molecular dynamics with attosecond resolution using correlated wave packet pairs *Nature* **421** 826

[66] Alnaser A S, Osipov T, Benis E P, Wech A, Shan B, Cocke C L, Tong X M and Lin C D 2003 Rescattering double ionization of D_2 and H_2 by intense laser pulses *Phys. Rev. Lett.* **91** 163002

[67] Mairesse Y *et al* 2003 Attosecond synchronization of high-harmonic soft x-rays *Science* **302** 1540

[68] Friedrich B and Herschbach D 1995 Alignment and trapping of molecules in intense laser fields *Phys. Rev. Lett.* **74** 4623

[69] Sakai H, Safvan C P, Larsen J J, Hilligs K M, Hald K and Stapelfeldt H 1999 Controlling the alignment of neutral molecules by a strong laser field *J. Chem. Phys.* **110** 10235

[70] Villeneuve D M, Aseyev S A, Dietrich P, Spanner M, Ivanov M Yu and Corkum P B 2000 Forced molecular rotation in an optical centrifuge *Phys. Rev. Lett.* **85** 542

[71] Underwood J G, Spanner M, Ivanov M Yu, Mottershead J, Sussman B J and Stolow A 2003 Switched wave packets: a route to nonperturbative quantum control *Phys. Rev. Lett.* **90** 223001

[72] Larsen J J, Hald K, Bjerre N, Stapelfeldt H and Seideman T 2000 Three dimensional alignment of molecules using elliptically polarized laser fields *Phys. Rev. Lett.* **85** 2470

[73] Sakai H, Minemoto S, Nanjo H, Tanji H and Suzuki T 2003 Controlling the orientation of polar molecules with combined electrostatic and pulsed, nonresonant laser fields *Phys. Rev. Lett.* **90** 083001

[74] Dooley P W, Litvinyuk I V, Lee K F, Rayner D M, Spanner M, Villeneuve D M and Corkum P B 2003 Direct imaging of rotational wave-packet dynamics of diatomic molecules *Phys. Rev.* A **68** 23406

[75] Bhardwaj V R, Rayner D M, Villeneuve D M and Corkum P B 2001 Quantum interference effects in double ionization and fragmentation of c_6h_6 *Phys. Rev. Lett.* **87** 417

[76] Litvinyuk I V, Lee K F, Dooley P W, Rayner D M, Villeneuve D M and Corkum P B 2003 Alignment-dependent strong field ionization of molecules *Phys. Rev. Lett.* **90** 233003

[77] Dinu L C, Muller H G, Kazamias S, Mullot G, Augé F, Balcou Ph, Paul P M, Kovaĉev M, Breger P and Agostini P 2003 Measurement of the subcycle timing of attosecond xuv bursts in high-harmonic generation *Phys. Rev. Lett.* **91** 063901

[78] Kak A C and Slaney M 2001 *Principles of Computerized Tomographic Imaging* (New York: Society for Industrial and Applied Mathematics)

[79] Niikura H, Villeneuve D M and Corkum P B 2005 Mapping attosecond electron wave packet motion *Phys. Rev. Lett.* **94** 083003

[80] Litvinyuk I V, Légaré F, Dooley P W, Villeneuve D M, Corkum P B, Zanghellini J, Pegarkov A, Fabian C and Brabec T 2005 Shakeup excitation during optical tunnel ionization *Phys. Rev. Lett.* **94** 033003

[81] Dörner R, Mergel V, Jagutzki O, Spielberger L, Ullrich J, Moshammer R and Schmidt-Böcking H 2000 Cold target recoil ion momentum spectroscopy: a 'momentum microscope' to view atomic collision dynamics *Phys. Rep.* **330** 95

[82] Paul P M, Toma E S, Breger P, Mullot G, Auge F, Balcou Ph, Muller H G and Agostini P 2001 Observation of a train of attosecond pulses from high harmonic generation *Science* **292** 1689–92

[83] Véniard V, Taïeb R and Maquet A 1996 Phase dependence of (n+1)-color (n>1) IR–UV photoionization of atoms with higher harmonics *Phys. Rev.* A **54** 721–8

[84] Jones D J, Diddams S A, Ranka J K, Stentz A, Windeler R S, Hall J L and Cundiff S T 2000 Carrier-envelope phase control of femtosecond mode-locked lasers and direct optical frequency synthesis *Science* **288** 635

[85] Poppe A, Holzwarth R, Apolonski A, Tempea G, Spielmann Ch, Hänsch T W and Krausz F 2001 Few-cycle optical waveform synthesis *Appl. Phys.* B **72** 373–6

[86] Ranka J, Windeler R and Stentz A 2000 *Opt. Lett.* **25** 25–7

[87] Fortier T M, Jones D J and Cundiff S T 2003 *Opt. Lett.* **28** 2198

[88] Morgner U, Ell R, Metzler G, Schibli T R, Kaertner F X, Fujimoto J G, Haus H A and Ippen E P 2001 *Phys. Rev. Lett.* **86** 5462–5

[89] Diddams S A, Jones D J, Ye J, Cundiff S T, Hall J L, Ranka J K, Windeler R S, Holzwarth R, Udem Th and Hänsch T W 2000 Direct link between microwave and optical frequencies with a 300 THZ femtosecond laser comb *Phys. Rev. Lett.* **84** 5102–5

[90] Toma E S, Muller H G, Paul P M, Breger P, Cheret M, Agostini P, Le Blanc C, Mullot G and Cheriaux G 2000 Ponderomotive streaking of the ionization potential as a method for measuring pulse durations in the XUV domain with fs resolution *Phys. Rev.* A **62** 061801

[91] Schins J M, Breger P, Agostini P, Constantinescu R C, Muller H G, Grillon G, Antonetti A and Mysyrowicz A 1994 Observation of laser-assisted Auger decay in argon *Phys. Rev. Lett.* **73** 2180

[92] Schins J M, Breger P, Agostini P, Constantinescu R C, Muller H G, Bouhal A, Grillon G, Antonetti A and Mysyrowicz A 1996 Cross-correlation measurements of femtosecond extreme-ultraviolet high-order harmonics *J. Opt. Soc. Am.* B **13** 197

[93] Glover T E, Schoenlein R W, Chin A H and Shank C V 1996 Observation of laser assisted photoelectric effect and femtosecond high order harmonic radiation *Phys. Rev. Lett.* **76** 2468

[94] Bouhal A, Evans R, Grillon G, Mysyrowicz A, Breger P, Agostini P, Constantinescu R-C, Muller H-G and von der Linde D 1997 Cross-correlation measurement of femtosecond noncollinear high-order harmonics *J. Opt. Soc. Am.* B **14** 950–6

[95] Christov I P, Murnane M M and Kapteyn H C 1997 High-harmonic generation of attosecond pulses in the 'single-cycle' regime *Phys. Rev. Lett.* **78** 1251–4

[96] Ivanov M, Corkum P B, Zuo T and Bandrauk A 1995 Routes to control of intense-field atomic polarizability *Phys. Rev. Lett.* **74** 2933–6

[97] Kim K T, Kim C M, Baik M G, Umesh G and Nam C H 2004 Single sub-50-attosecond pulse generation from chirp-compensated harmonic radiation using material dispersion *Phys. Rev.* A **69** 051805

[98] Kitzler M, Milosevic N, Scrinzi A, Krausz F and Brabec T 2002 Quantum theory of attosecond XUV pulse measurement by laser dressed photoionization *Phys. Rev. Lett.* **88** 173904
[99] Belenov E M, Nazarkin A V and Prokopovich I P 1992 Dynamics of an intense femtosecond pulse in a Raman-active medium *Sov. Phys.—JETP Lett.* **55** 218–22
[100] Belenov E M, Kryukov P G, Nazarkin A V and Prokopovich I P 1994 Propagation dynamics of high-power femtosecond pulses in Raman-active media *Sov. Phys.—JETP* **78** 15–22
[101] Prokopovich I P and Khrushchinskii A A 1997 Highly efficient generation of attosecond pulses in coherent stimulated Raman self-scattering of intense femtosecond laser pulses *Laser Phys.* **7** 305
[102] Yoshikawa S and Imasaka T 1993 A new approach for the generation of ultrashort optical pulses *Opt. Commun.* **96** 94
[103] Harris S E and Sokolov A V 1998 Subfemtosecond pulse generation by molecular modulation *Phys. Rev. Lett.* **81** 2894–7
[104] Kawano H, Hirakawa Y and Imasaka T 1998 Generation of high-order rotational lines in hydrogen by four-wave Raman mixing in the femtosecond regime *IEEE J. Quantum Electron.* **34** 260–8
[105] Hakuta K, Suzuki M, Katsuragawa M and Li Z 1997 Self-induced phase matching in parametric anti-Stokes stimulated Raman scattering *Phys. Rev. Lett.* **58** 209–12
[106] Li J Z, Katsuragawa M, Suzuki M and Hakuta K 1998 Stimulated Raman scattering in solid hydrogen: measurement of coherence decay *Phys. Rev.* A **58** R58–R60
[107] Sokolov A V, Walker D R, Yavuz D D, Yin G Y and Harris S E 2000 Raman generation by phased and antiphased molecular states *Phys. Rev. Lett.* **85** 562–5
[108] Kaplan A E 1994 Subfemtosecond pulses in mode-locked 2 pi solitons of the cascade stimulated Raman scattering *Phys. Rev. Lett.* **73** 1243–6
[109] Yavuz D D, Sokolov A V and Harris S E 2000 Eigenvectors of a Raman medium *Phys. Rev. Lett.* **84** 75–8
[110] Sokolov A V, Walker D R, Yavuz D D, Yin G Y and Harris S E 2001 Femtosecond light source for phase-controlled multiphoton ionization *Phys. Rev. Lett.* **87** 033402
[111] Yavuz D D, Walker D R, Yin G Y and Harris S E 2002 Rotational Raman generation with near-unity conversion efficiency *Opt. Lett.* **27** 769–71
[112] Yavuz D D, Walker D R, Shverdin M Y, Yin G Y and Harris S E 2003 Quasiperiodic Raman technique for ultrashort pulse generation *Phys. Rev. Lett.* **91** 233602
[113] Wittmann M, Nazarkin A and Korn G 2000 Fs-pulse synthesis using phase modulation by impulsively excited molecular vibrations *Phys. Rev. Lett.* **84** 5508–11
[114] Wittmann M, Nazarkin A and Korn G 2001 Synthesis of periodic femtosecond pulse trains in the ultraviolet by phase-locked Raman sideband generation *Opt. Lett.* **26** 298–300
[115] Zhavoronkov N and Korn G 2002 Generation of single intense short optical pulses by ultrafast molecular phase modulation *Phys. Rev. Lett.* **88** 203901
[116] Nazarkin A, Korn G, Wittmann M and Elsaesser T 2002 Group-velocity-matched interactions in hollow waveguides: enhanced high-order Raman scattering by impulsively excited molecular vibrations *Phys. Rev.* A **65** 041802
[117] Bartels R A, Weinacht T C, Wagner N, Baertschy M, Greene C H, Murnane M M and Kapteyn H C 2002 Phase modulation of ultrashort light pulses using molecular rotational wave packets *Phys. Rev. Lett.* **88** 013903
[118] Sali E, Mendham K J, Tisch J W G, Halfmann T and Marangos J P 2004 High-order stimulated Raman scattering in a highly transient regime driven by a pair of ultrashort pulses *Opt. Lett.* **29** 495–7
[119] Sali E, Kinsler P, New G H C, Mendham K J, Halfmann T, Tisch J W G and Marangos J P 2005 Behavior of high-order stimulated Raman scattering in a highly transient regime *Phys. Rev.* A **72** 013813
[120] Gundry S, Anscombe M P, Abdulla A M, Sali E, Tisch J W G, Kinsler P, New G H C and Marangos J P 2005 Ultrashort-pulse modulation in adiabatically prepared Raman media *Opt. Lett.* **30** 180–2
[121] Kalosha V, Spanner M, Herrmann J and Ivanov M 2002 Generation of single dispersion precompensated 1-fs pulses by shaped-pulse optimized high-order stimulated Raman scattering *Phys. Rev. Lett.* **88** 103901
[122] Spanner M and Ivanov M Yu 2003 Optimal generation of single-dispersion precompensated 1-fs pulses by molecular phase modulation *Opt. Lett.* **28** 576
[123] Nguyen Hong Shon, Le Kien F, Hakuta K and Sokolov A V 2002 Two-dimensional model for femtosecond pulse conversion and compression using high-order stimulated Raman scattering in solid hydrogen *Phys. Rev.* A **65** 033809
[124] Kalosha V P and Herrmann J 2003 Ultrawide spectral broadening and compression of single extremely short pulses in the visible and UV–VUV and middle infrared by high-order stimulated raman scattering *Phys. Rev.* A **68** 023812
[125] Kalosha V P and Herrmann J 2003 Compression of single-cycle mid-infrared pulses by Raman-active molecular modulators *Opt. Lett.* **28** 950–2

[126] Sokolov A V, Shverdin M Y, Walker D R, Yavuz D D, Burzo A M, Yin G Y and Harris S E 2005 Generation and control of femtosecond pulses by molecular modulation *J. Mod. Opt.* **52** 285–304
[127] Harris S E, Walker D R and Yavuz D D 2002 Raman technique for single-cycle pulses *Phys. Rev.* A **65** 021801
[128] Burzo A M and Sokolov A V 2004 Generation of single-cycle pulses spaced by an integer number of molecular periods *J. Mod. Opt.* **51** 2665–73
[129] Kalosha V P and Herrmann J 2000 Phase relations and quasicontinuous spectra and subfemtosecond pulses in high-order stimulated Raman scattering with short-pulse excitation *Phys. Rev. Lett.* **85** 001226
[130] Durfee C G III, Rundquist A R III, Herne C, Backus S, Murnane M M and Kapteyn H C 1999 Phase matching of high-order harmonics in hollow waveguides *Phys. Rev. Lett.* **83** 2187–90
[131] Constant E, Garzella D, Breger P, Mevel E, Dorrer Ch, Le Blanc C, Salin F and Agostini P 1999 Optimizing high harmonic generation in absorbing gases: model and experiment *Phys. Rev. Lett.* **82** 1668–71
[132] Roos L, Constant E, Mevel E, Balcou P, Descamps D, Gaarde M B, Valette A, Haroutunian R and L'Huillier A 1999 Controlling phase matching of high-order harmonic generation by manipulating the fundamental field *Phys. Rev.* A **60** 5010–8
[133] Takahashi E, Nabekawa Y, Otsuka T, Obara M and Midorikawa K 2002 Generation of highly coherent submicrojoule soft x rays by high-order harmonics *Phys. Rev.* A **66** 021802
[134] Altucci C *et al* 2003 Phase-matching analysis of high-order harmonics generated by truncated Bessel beams in the sub-10-fs regime *Phys. Rev.* A **68** 033806
[135] Takahashi E, Tosa V, Nabekawa Y and Midorikawa K 2003 Experimental and theoretical analyses of a correlation between pump–pulse propagation and harmonic yield in a long-interaction medium *Phys. Rev.* A **68** 023808
[136] Tosa V, Takahashi E, Nabekawa Y and Midorikawa K 2003 Generation of high-order harmonics in a self-guided beam *Phys. Rev.* A **67** 063817
[137] Naumova N M, Nees J A, Sokolov I V, Hou B and Mourou G A 2004 Relativistic generation of isolated attosecond pulses in a lambda 3 focal volume *Phys. Rev. Lett.* **92** 063902
[138] Naumova N, Sokolov I, Nees J, Maksimchuk A, Yanovsky V and Mourou G 2004 Attosecond electron bunches *Phys. Rev. Lett.* **93** 195003
[139] Gordienko S, Pukhov A, Shorokhov O and Baeva T 2004 Relativistic Doppler effect: universal spectra and zeptosecond pulses *Phys. Rev. Lett.* **93** 115002
[140] Nees J *et al* 2005 Relativistic generation of isolated attosecond pulses: a different route to extreme intensity *J. Mod. Opt.* **52** 305–19
[141] Bulanov S V, Naumova N M and Pegoraro F 1994 Interaction of an ultrashort, relativistically strong laser pulse with an overdense plasma *Phys. Plasmas* **1** 745–57
[142] Vshivkov V A, Naumova N M, Pegoraro F and Bulanov S V 1998 Nonlinear electrodynamics of the interaction of ultra-intense laser pulses with a thin foil *Phys. Plasmas* **5** 2727–41
[143] Lichters R, Meyer ter Vehn J and Pukhov A 1996 Short-pulse laser harmonics from oscillating plasma surfaces driven at relativistic intensity *Phys. Plasmas* **3** 3425–37
[144] von der Linde D and Rzazewski K 1996 High-order optical harmonic generation from solid surfaces *Appl. Phys.* B **63** 499–506
[145] Plaja L, Roso L, Rzazewski K and Lewenstein M 1998 Generation of attosecond pulse trains during the reflection of a very intense laser on a solid surface *J. Opt. Soc. Am.* **15** 1904–11
[146] Leitenstorfer A, Furst C and Laubereau A 1995 Widely tunable two-color mode-locked Ti:sapphire laser with pulse jitter of less than 2 fs *Opt. Lett.* **20** 916–8
[147] Wei Z, Kobayashi Y, Zhang Z and Torizuka K 2001 Generation of two-color femtosecond pulses by self-synchronizing Ti–sapphire and Cr–forsterite lasers *Opt. Lett.* **26** 1806–8
[148] Betz M, Sotier F, Tauser F, Trumm S and Laubereau A 2004 All-optical phase locking of two femtosecond Ti:sapphire lasers: a passive coupling mechanism beyond the slowly varying amplitude approximation *Opt. Lett.* **29** 629–31
[149] Ma L S, Shelton R K, Kapteyn H C, Murnane M M and Ye J 2001 Sub-10-femtosecond active synchronization of two passively mode-locked Ti:sapphire oscillators *Phys. Rev.* A **64** 021802
[150] Shelton R K, Foreman S M, Ma L S, Hall J L, Kapteyn H C, Murnane M M, Notcutt M and Ye J 2002 Subfemtosecond timing jitter between two independent, actively synchronized, mode-locked lasers *Opt. Lett.* **27** 312–4
[151] Schibli T R, Kim J, Kozucu O, Gopinath J T, Tandon S N, Petrich G S, Koloziejski L A, Fujimoto J G, Ippen E P and Kaertner F X 2003 Attosecond active synchronization of passively mode-locked lasers by balanced cross correlation *Opt. Lett.* **28** 947–9
[152] Shelton R K, Ma L S, Kapteyn H C, Murnane M M, Hall J L and Ye J 2001 Phase-coherent optical pulse synthesis from separate femtosecond lasers *Science* **293** 1286–9

[153] Rauschenberger J, Fortier T M, Jones D J, Ye J and Cundiff S T 2002 Control of the frequency comb from a mode-locked erbium-doped fiber laser *Opt. Express* **10** 1404–10
[154] Kobayashi Z, Wei Z Y, Kakehata M, Takada H and Torizuka K 2003 Relative carrier-envelope-offset phase control between independent femtosecond light sources *IEEE J. Quantum Electron.* **9** 1011–7
[155] Ihee H, Lobastov V A, Gomez U M, Goodson B M, Srinivasan R, Ruan C-Yu and Zewail A H 2001 Direct imaging of transient molecular structures with ultrafast diffraction *Science* **291** 458
[156] Siwick B J, Dwyer J R, Jordan R E and Miller R J D 2003 An atomic-level view of melting using femtosecond electron diffraction *Science* **302** 5649
[157] Zuo T, Bandrauk A D and Corkum P B 1996 Laser-induced electron diffraction: a new tool for probing ultrafast molecular dynamics *Chem. Phys. Lett.* **259** 313
[158] Lein M, Marangos J P and Knight P L 2002 Electron diffraction in above-threshold ionization of molecules *Phys. Rev.* A **66** 051404
[159] Lein M, Hay N, Velotta R, Marangos J and Knight P 2002 Interference effects in high-order harmonic generation with molecules *Phys. Rev. Lett.* **88** 183903
[160] Yurchenko S N, Patchkovskii S, Litvinyuk I V, Corkum P B and Yudin G L 2004 Laser-induced interference, focusing, and diffraction of rescattering molecular photoelectrons *Phys. Rev. Lett.* **93** 223003
[161] Spanner M, Smirnova O, Corkum P and Ivanov M 2004 Reading diffraction images in strong field ionization of diatomic molecules *J. Phys. B: At. Mol. Opt. Phys.* **37** L243
[162] Stapelfeldt H and Seideman T 2003 Colloquium: aligning molecules with strong laser pulses *Rev. Mod. Phys.* **75** 543
[163] Milosevic D B and Becker W 2000 Attosecond pulse trains with unusual nonlinear polarization *Phys. Rev.* A **62** 011403
[164] Milosevic D B, Becker W and Kopold R 2000 Generation of circularly polarized high-order harmonics by two-color coplanar field mixing *Phys. Rev.* A **61** 063403
[165] Spanner M, Smironova O and Scrinzi A 2005 Attosecond XUV probing of strong field ionization dynamics from one- and two-electron 1d atoms *High Field Attosecond Physics (Obergurgl, Austria, 9–15 Jan.)*
[166] Piraux B, Bauer J, Laulan S and Bachau H 2003 Probing electron–electron correlation with attosecond pulses *Eur. Phys. J.* D **26** 7
[167] Milosevic N, Corkum P B and Brabec T 2004 How to use lasers for imaging attosecond dynamics of nuclear processes *Phys. Rev. Lett.* **92** 013002
[168] Tzallas P, Charalambidis D, Papadogiannis N A, Witte K and Tsakiris G D 2003 Direct observation of attosecond light bunching *Nature* **426** 267–71
[169] Sekikawa T, Kosuge A, Kanai T and Watanabe S 2004 Non-linear optics in the extreme ultraviolet *Nature* **432** 602